

## Article

# Analysis of the Soft-Switching Tuning Effect on the Figures of Merit Involved in the Design of a Class-E Amplifier with Finite DC-Feed Inductance

Ingrid Casallas , Robert Urbina , Carlos-Ivan Paez-Rueda , Gabriel Perilla , Manuel Pérez   
and Arturo Fajardo \* 

Department of Electronic Engineering, Pontificia Universidad Javeriana, Bogotá 110311, Colombia; ingrid.casallas@javeriana.edu.co (I.C.); r\_urbina@javeriana.edu.co (R.U.); paez.carlos@javeriana.edu.co (C.-I.P.-R.); gabriel.perilla@javeriana.edu.co (G.P.); manuel.perez@javeriana.edu.co (M.P.)

\* Correspondence: fajardoa@javeriana.edu.co

**Abstract:** This paper explores the design of a Class-E amplifier with finite DC-feed inductance using three tuning methods. Furthermore, this work quantifies the impacts of the tuning process (referred to in this paper as the tuning effect) on the main figures of merit (FoMs) of this amplifier. The tuning goals were to guarantee two conditions: zero voltage and zero voltage derivative switching (i.e., soft-switching tuning). To the best of the authors' knowledge, systematic tuning methods have not been analyzed before for this amplifier topology. Two of them are based on the iterative component tuning process, and they have been explored previously in the design of the conventional class-E amplifier with an RF choke inductance. The last tuning method explores the simultaneous adjustment of the control signal period and one amplifier capacitor. The analyzed tuning methods were validated by extensive simulations of case studies, which were designed following the power specifications of the Qi standard. In 100% and 96% of the case studies, zero voltage switching (ZVS) and zero-derivative voltage switching (ZDS) were achieved, respectively. Furthermore, we identified an unexpected behavior in the tuning process (referred to in this paper as the turning point), which consisted of a change of the expected trend of the soft-switching (i.e., ZVS and ZDS) point, and it occurred in 21% of the case studies. When this behavior occurred and converged to at least ZVS, the tuning process required more iterations and a large number of tuning variables. Additionally, after the tuning process, the total harmonic distortion and output power capacity were improved (i.e., in 78% and 61% of the case studies, respectively), whereas the output power, drain and added power efficiencies deteriorated (i.e., in 83%, 61% and 65% of the case studies, respectively) in the overall case studies. However, we could not identify an improvement in the overall FoMs related to the soft-switching tuning. Furthermore, the tuning impact was significant and produced some improvements and some deleterious effects for the FoMs in each case study, without a clear trend by FoMs or by tuning method. Therefore, the amplifier designer may choose the more favorable tuning method and the related FoM trade-offs for the required design specifications.

**Keywords:** Class E; design methods; tuning; power amplifier



**Citation:** Casallas, I.; Urbina, R.; Paez-Rueda, C.I.; Perilla, G.; Pérez, M.; Fajardo, A. Analysis of the Soft-Switching Tuning Effect on the Figures of Merit Involved in the Design of a Class-E Amplifier with Finite DC-Feed Inductance. *Electronics* **2021**, *10*, 1705. <https://doi.org/10.3390/electronics10141705>

Academic Editor: Jianxing Liu

Received: 26 April 2021

Accepted: 5 June 2021

Published: 16 July 2021

**Publisher's Note:** MDPI stays neutral with regard to jurisdictional claims in published maps and institutional affiliations.



**Copyright:** © 2021 by the authors. Licensee MDPI, Basel, Switzerland. This article is an open access article distributed under the terms and conditions of the Creative Commons Attribution (CC BY) license (<https://creativecommons.org/licenses/by/4.0/>).

## 1. Introduction

Class-E power amplifiers (PA) are used in many RF applications, such as biotelemetry [1], plasma generation [2], wireless power transmission [3,4], dedicated short-range communications [5], magnetic resonant imaging [6], induction heater systems [7] and street-lighting [8]. This PA is attractive in applications that demand high power consumption, because it achieves a theoretical power efficiency of 100%. Its circuit topology is shown in Figure 1. It consists of a single switch ( $S_W$ ) controlled by a periodic signal ( $v_{in}$ ), a DC power source ( $V_{DD}$ ) in series with an inductor ( $L_{SH}$ ), a shunt capacitor ( $C_{SH}$ ) and

a resonant network (i.e.,  $L_o$ ,  $C_e$  and  $R_L$ ). In the nominal operation,  $S_W$  satisfies the zero voltage switching (ZVS) and zero voltage derivative switching (ZVDS) conditions, which reduces the switching losses [9]. This ideal soft-switching behavior is shown in Figure 2.

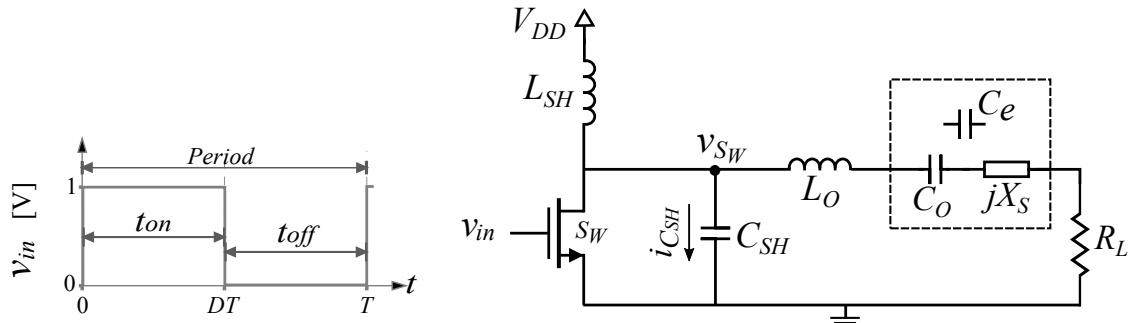


Figure 1. Ideal model of the class-E PA with finite DC-feed inductance.

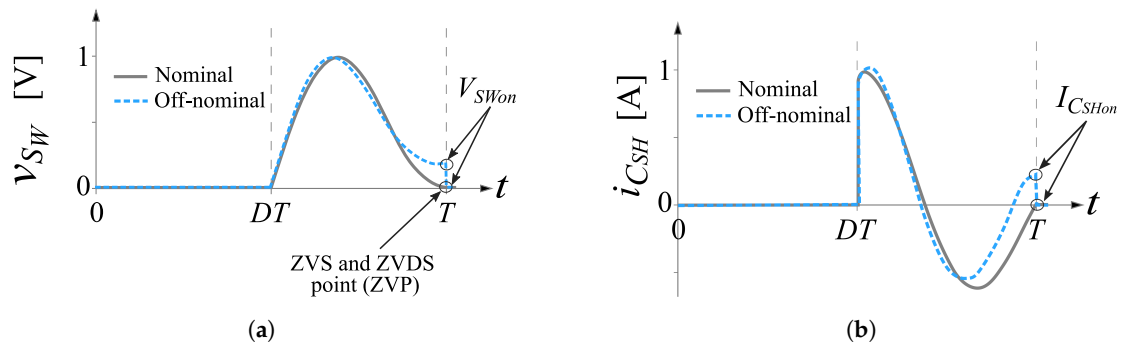


Figure 2. Normalized nominal and off-nominal waveforms of the class-E amplifier. (a)  $C_{SH}$  voltage. (b)  $C_{SH}$  current.

The design of the class-E PA has been explored in several works [9–24]. From the point of view of the  $L_{SH}$  element, the class-E PA can be divided into two topologies: class-E PA with RF choke [9–12] and class-E PA with finite DC-feed inductance (FDI) [13–24]. The model of a class-E PA with RF choke assumes a DC input current, which simplifies the mathematical analysis and allows its design through simple analytical equations [9,12]. In contrast, the class-E PA with FDI must consider the current waveform in the circuit analysis, which increases the complexity of the design [19,23]. However, the finite feed inductance increases the designer's degrees of freedom. For instance, the designer of a class-E PA with FDI must optimize the component combination to achieve the design specifications and restrictions with high-efficiency [23,24]. Additionally, FDI is particularly useful in applications with size constraints, because it allows inductors to be reduced in size [18,21].

The ideal class-E with FDI assumes components with infinitely high quality factors (i.e., without parasitic elements), and a switch with zero rise and fall commutation times and zero on-resistance [19,23]. Following these assumptions, this ideal amplifier achieves high efficiency under the ZVS and ZVDS conditions. However, these design assumptions are not reached with real components because the parasitic elements significantly affect the soft-switching conditions. Therefore, the efficiency and other figures of merit (FoMs) are affected in the practical implementations [25].

Commonly, the PA design starts with the calculation of the initial circuit component values through design equations [9,12,19,22–24,26]. However, these equations only provide an approximation of the nominal class-E operation (i.e., ZVS and ZVDS) because of the parasitic elements. A common solution to guarantee the soft-switching operation with parasitic elements is component tuning [10,12,21,23,24,27–29]. However, and to the best of the authors' knowledge, this method has not been analyzed in class-E PAs with FDI topology. In particular, different tuning methods have been reported [12,26] for the conventional class-E PA (i.e., with RF choke). In [26], the effects of adjusting the load-network components were described (i.e.  $R_L$ ,  $C_{SH}$ ,  $C_e$  and  $L_o$ ), and a tuning procedure that adjusts

$C_{SH}$  and  $C_e$  was proposed. Recently, this tuning approach has been explored in wireless power transfer systems to improve their efficiency [4,28,29]. Additionally, in [12] a tuning process that alters  $L_{SH}$  and  $C_{SH}$  was reported, based on the design equations reported in [9]. The effects of the component variations on the ZVS and ZVDS point (ZVP) of the conventional class-E PA are shown in Figure 3.

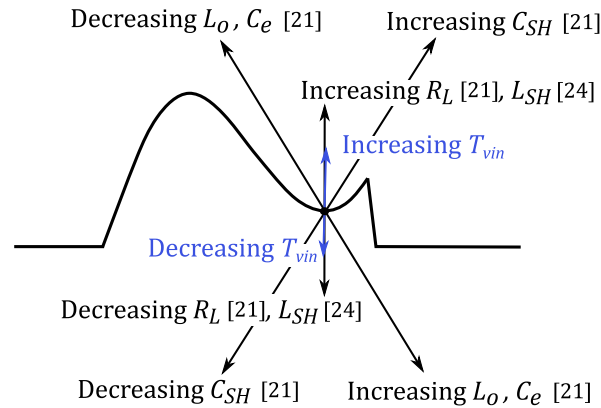


**Figure 3.** Effects of the component variations on the ZVP [12,26].

Non-soft-switching [27] and soft-switching tuning techniques [4,12,26,28,29] have been explored for designing class-E PAs with RF choke. The soft-switching tuning guarantees the nominal amplifier waveforms, which are shown in Figure 2. In a class-E PA with RF choke, this nominal operation implies maximum efficiency only if the parasitic elements are negligible. Furthermore, the maximum PA efficiency is achieved with an off-nominal waveform, which is related to the values of the parasitic elements [30]. For instance, in [31], the authors found that the conventional class-E amplifier operates with maximum efficiency if its switch turn-on voltage ( $V_{SWon}$ ) is in the range of 10% to 50% of the  $V_{DD}$ . This is because the increase of the power loss in the switch element is smaller than the decrease of the power dissipation by the parasitic elements, and consequently, the total power dissipation is minimized in the amplifier [31]. The switching losses increase because the energy stored by  $C_{SH}$  is dissipated upon switch turn-on, and the power losses of the parasitic elements decrease because the PA current waveforms change slightly. However, in this conventional amplifier, the soft-switching tuning guarantees the reduction of the current spikes and switching losses, which can prolong the components' lifetimes and decrease the electromagnetic interference [32]. These soft-switching tuning techniques could be involved in the design of a class-E PA with FDI. Furthermore, to the best of the authors' knowledge, these techniques have not been used or analyzed in regard this amplifier topology.

In this paper, we analyze the effects of soft-switching tuning on the main FoMs of a class-E PA with FDI. Furthermore, we propose a design methodology based on an ideal model of the class-E PA with FDI [23,24], a specific design created for maximum output power [18] and three soft-switching tuning methods. Two of them are based on the iterative component tuning process, and they have been explored previously in the design of the conventional class-E amplifier [12,26]. The last tuning technique explores variations of the  $v_{in}$  period ( $T_{vin}$ ) and the  $C_{SH}$  capacitor. The presented tuning methods were validated through eight different case studies with specifications based on the Qi standard [33]. Additionally, this paper introduces the turning point concept, which is an unexpected behavior of the tuning process. The turning point consists of a change of the expected trend of the soft-switching point (i.e., ZVS and ZDS), as we detail in Section 3. When the tuning process converges to at least ZVS, it requires more iterations and a long number of tuning variables. The rest of the article is divided as follows. Section 2 describes the proposed design methodology and the tuning methods. Section 3 presents the case studies and their simulation results. Section 4 summarizes the analysis of results. Finally, Sections 5 and 6 present the future work and the conclusions, respectively.

## 2. Proposed PA Design Methodology

The PA design methodology proposed in this paper involves three steps. In the first step, the component values of the ideal class-E PA with FDI are calculated. In the second step, a simulation with non-ideal components is performed to verify the design specifications and the PA operating conditions. Finally, in the third step, a tuning process is implemented to reach nominal class-E-level operation (i.e., ZVS and ZVDS). This last step considers three different tuning methods. Two of them have been previously explored in the design of the conventional class-E PA (i.e., with an RF choke inductor). The third explores the variations of  $T_{v_{in}}$  and  $C_{SH}$ . These design steps are detailed below.

### 2.1. Design of the Ideal Amplifier

This step implies, first, calculating the component values of the ideal class-E PA with FDI through a reported amplifier model [12,18–20]. Second comes choosing the most suitable model according to the designer's experience or mathematical implementations. This step only provides a starting point for the component values. Therefore, a high-complexity model can result in unnecessary wasting of time and resources.

In this document, we use the well-known ideal class-E with FDI model reported in [19]. This model assumes a high-loaded quality factor ( $Q_L$ ) of the resonant circuit, and consequently a pure sinusoidal signal across  $R_L$ . Under these assumptions, the PA circuit model is simplified to the one shown in Figure 4. The analysis of this simplified circuit model resulted in five analytical design equations. These equations are grouped in a design set:  $K = K_L, K_C, K_P, K_X$  and  $K_{Q_L}$ . Those are the PA specifications for the PA circuit components [19,23]. According to the model reported in [19,23], the design set was composed of analytical functions of two model parameters, the duty cycle ( $D$ ) and the resonance frequency mismatch ( $q$ ), which are given by:

$$K_L(D, q) = \frac{\omega_o L_{SH}}{R_L} \quad (1)$$

$$K_C(D, q) = \omega_o C_{SH} R_L \quad (2)$$

$$K_P(D, q) = \frac{P_{out} R_L}{V_{DD}^2} \quad (3)$$

$$K_X(D, q) = \frac{X_s}{R_L} \quad (4)$$

$$K_{Q_L} = Q_L = \frac{\omega_o L_o}{R_L} = \frac{1}{\omega_o C_o R_L} \quad (5)$$

where  $\omega_o$  is the angular operating frequency and  $X_s$  is an inductive or capacitive reactance that must be added to the resonant network (i.e.,  $L_o$  and  $C_o$ ) to guarantee the PA operation under soft-switching conditions. In [19], the authors showed that assuming a  $D = 0.5$ , the output power is maximized with  $q = 1.412$ , which results in the design set summarized in Table 1. This design set is used to calculate the initial component values of the case studies developed in Section 3.

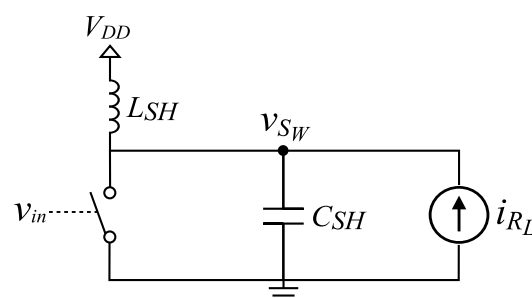


Figure 4. Ideal model of the class-E PA with finite DC-feed inductance [23].

**Table 1.** Design set values for  $D = 0.5$  and  $q = 1.412$  [23].

Parameter	$K_L$	$K_C$	$K_P$	$K_X$
Value	0.7332	0.6841	1.363	-0.0001716

### 2.2. Evaluation of the Amplifier with Non-Ideal Components

In this step, the designer must evaluate the designed PA via simulation using the components calculated in the first step and include at least the equivalent series resistance (ESR) of the coils and capacitors and the switch model (i.e., the transistor simulation model). The ESR can be estimated from commercial values or calculated from a given component quality factor. Once the simulation is carried out, it must verify compliance with the design specifications by the measuring of some FoMs (e.g., efficiency and THD) and the analyzing of the simulation results. Finally, the designer must check the soft-switching operation by the  $V_{SWon}$  and the  $I_{C_{SHon}}$ .

### 2.3. Design for Soft-Switching Operation via a Tuning Process

The tuning method consists of moving the ZVP to achieve the ZVS and ZVDS conditions. Generally, the ZVP is moved by adjusting the values of two components, which oppositely affect the ZVP. For instance, one component changes the ZVP vertically, and the other changes the ZVP horizontally. Consequently, the tuning process requires changing the values of the two elements until reaching the soft-switching conditions within a tolerance margin. This tuning process can be used in simulations or in prototyped circuits. In the simulation, the tuning can be performed by parametric sweeps of the involved component values. On the other hand, in a prototyped amplifier, the tuning can be performed by component replacements.

#### 2.3.1. Tuning Method 1 (TM1): Adjustment of $C_{SH}$ and $L_{SH}$

This tuning method was proposed in [12] for class-E PAs with RF choke. It involves adjustments of  $C_{SH}$  and  $L_{SH}$  to reach the nominal class-E operation. The effects of these two components on the ZVP point are observed in Figure 5a. In this tuning method, the ZVP point is adjusted horizontally through  $C_{SH}$  variations and vertically by  $L_{SH}$  variations.

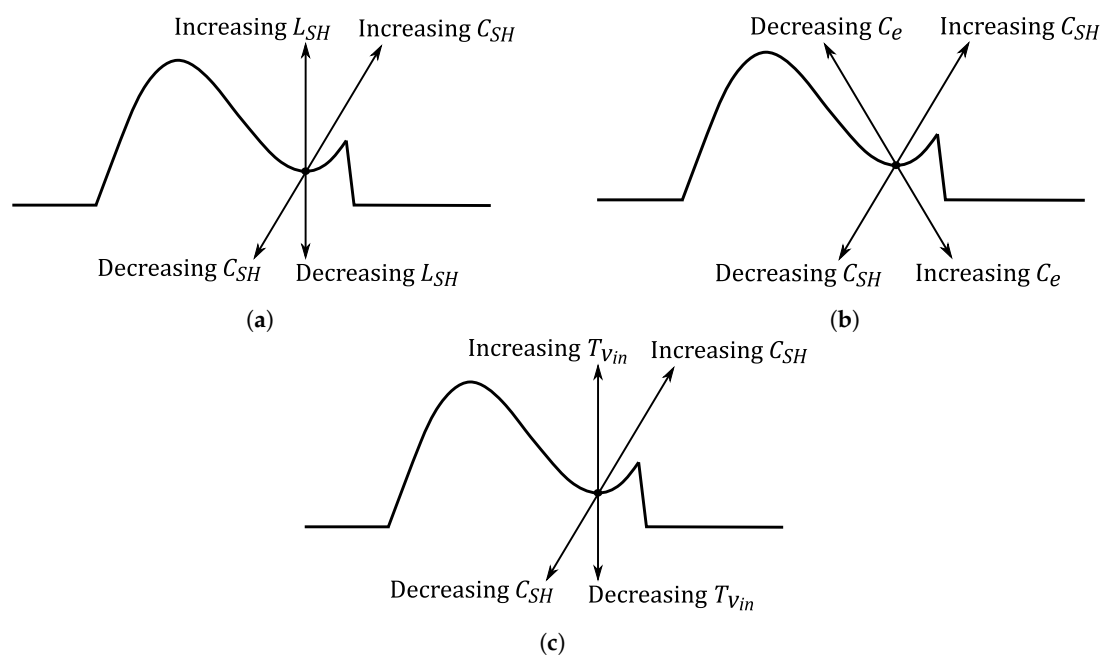


**Figure 5.** Effects of component variations on the ZVP (a) Tuning method 1:  $C_{SH}$  and  $L_{SH}$  variations [12]. (b) Tuning method 2:  $C_{SH}$  and  $C_e$  variations [26]. (c) Tuning method 3:  $C_{SH}$  and  $T_{vin}$  variations.

### 2.3.2. Tuning Method 2 (TM2): Adjustment of $C_{SH}$ and $C_e$

This tuning method was proposed by Sokal in [26] for class-E PAs with RF choke. It involves adjustments of  $C_e$  and  $C_{SH}$  to reach nominal class-E operation. The effects of these components on the ZVP point are shown in Figure 5b. In this tuning method, the ZVP point is affected horizontally and vertically by the two components. Therefore, the tuning process will depend on the specific design case.

### 2.3.3. Tuning Method 3 (TM3): Adjustment of $C_{SH}$ and $T_{v_{in}}$

As an alternative to the conventional soft-switching tuning methods, this new approach allows achieving nominal operation with the tuning of only one circuit component of a class-E PA with FDI. This feature is particularly useful in circuit implementations that use an adjustable digital signal for  $v_{in}$ . The  $T_{v_{in}}$  effect on the ZVP is shown in Figure 5c. Similarly to tuning method 1, the ZVP point is adjusted horizontally and vertically by the  $C_{SH}$  and  $T_{v_{in}}$  variations, respectively.

## 3. Case Studies and Results

The proposed design methodology was validated through eight case studies of a class-E PA with FDI, whose power specifications were taken from the Qi standard [33]. This standard defines inductive charging guides for wireless power applications over short distances (i.e., up to 4 cm). The specifications of the proposed case studies are listed in Table 2. The frequencies and output power were 87–205 kHz and 5–15 W; these ranges are defined by the Qi standard [34]. Additionally, the input voltage was defined based on the typical values used by charging stands and AC adapters (i.e., 5 and 12 V, which are USB and automotive power, respectively). Furthermore, the overall amplifiers used a commercial transmitter coil of 24  $\mu\text{H}$  with an ESR of 72 m $\Omega$  as the  $L_o$  component [35]. Moreover, these case studies cover a wide range of variables, which allows evaluating the tuning methods described in the design methodology extensively.

**Table 2.** Specifications of the class-E PA. footer \* All case studies were designed with  $D = 0.5$  and  $L_o = 24.0 \mu\text{H}$ .

Case Study *	Frequency [kHz]	$V_{DD}$ [V]	$P_{out}$ [W]
1	100	5.00	5.00
2	100	5.00	15.0
3	100	12.0	5.00
4	100	12.0	15.0
5	200	5.00	5.00
6	200	5.00	15.0
7	200	12.0	5.00
8	200	12.0	15.0

Following the methodology described in Section 2, the resulting component values of the ideal class-E PA with FDI are shown in Table 3. These values were found using the design tools developed in [23]. Additionally, we considered the ESR of each component in the simulation of a class-E PA with FDI. These resistances were calculated using typical values (i.e., quality factors of 200 and 80 for capacitors and the  $L_{SH}$  inductor, respectively [36]). The resulting ESR values are summarized in Table 3.

The evaluation of the designed class-E PAs was performed by circuit simulations in OrCAD PSpice® Designer software. All simulations used components with their respective ESRs; a  $v_{in}$  signal with zero falls and rise commutation times; and a commercial MOSFET (i.e., IPI029N06N) as the switch element. The PSpice simulation was carried out using a MOSFET Spice-like model provided by the manufacturer, which is shown in Figure 6. This model is a semi-empirical, short-channel model based on a native PSpice MOSFET (Level 3) [37]. This model was chosen because it exhibits a smooth and continuous transition between the weak and strong inversion region, and in the region between linear and saturation modes of device

operation [38]. Furthermore, this quasi-empirical model is characterized by low complexity, which implies short simulation times. Consequently, the manufacturer recommends this model to general electrical simulations for whole application circuits [39]. The transient analysis used a maximum time step of 0.5 ns and a simulation time of 3 to 5 ms. Additionally, the ideal amplifiers (i.e., without ESR and with an ideal switch) were simulated to examine the effects of the parasitic elements on the main class-E FoMs. These PA simulations used the same transient configuration; ideal components; a voltage-controlled switch with zero fall and rise times; an off-resistance of 1 GΩ; and an on-resistance of 1 mΩ. Furthermore, the FoMs examined in simulation were power added efficiency (PAE) ( $V_{SWon}$ ), drain efficiency ( $\eta = P_{out}/P_{VDD}$ ), input DC power ( $P_{VDD}$ ), output power ( $P_{out}$ ), total harmonic distortion (THD) and output power capability ( $C_p$ ), which is given by [25]

$$C_p = \frac{P_{out}}{I_{Smax} \cdot V_{Smax}} \tag{6}$$

where  $I_{Smax}$  and  $V_{Smax}$  are the maximum switch current and switch voltage values, respectively.

**Table 3.** Class-E PA component values with ESR.

Case Study	$L_{SH}$		$C_{SH}$		$C_e$		$R_L$ [Ω]	$Q_L$
	Value [μH]	ESR [mΩ]	Value [nF]	ESR [mΩ]	Value [nF]	ESR [mΩ]		
1	8.00	63.0	159.7	50.0	105.5	75.0	6.80	2.218
2	2.70	21.0	479.2	17.0	105.5	75.0	2.30	6.556
3	45.8	360	27.70	287	105.5	75.0	39.3	0.3837
4	15.3	120	83.20	96.0	105.5	75.0	13.1	1.151
5	4.00	31.0	79.90	100	26.40	301	6.80	4.435
6	1.30	10.0	239.6	33.0	26.40	301	2.30	13.11
7	22.9	180	13.90	572	26.40	301	39.3	0.7674
8	7.60	60.0	41.60	191	26.40	301	13.1	2.302

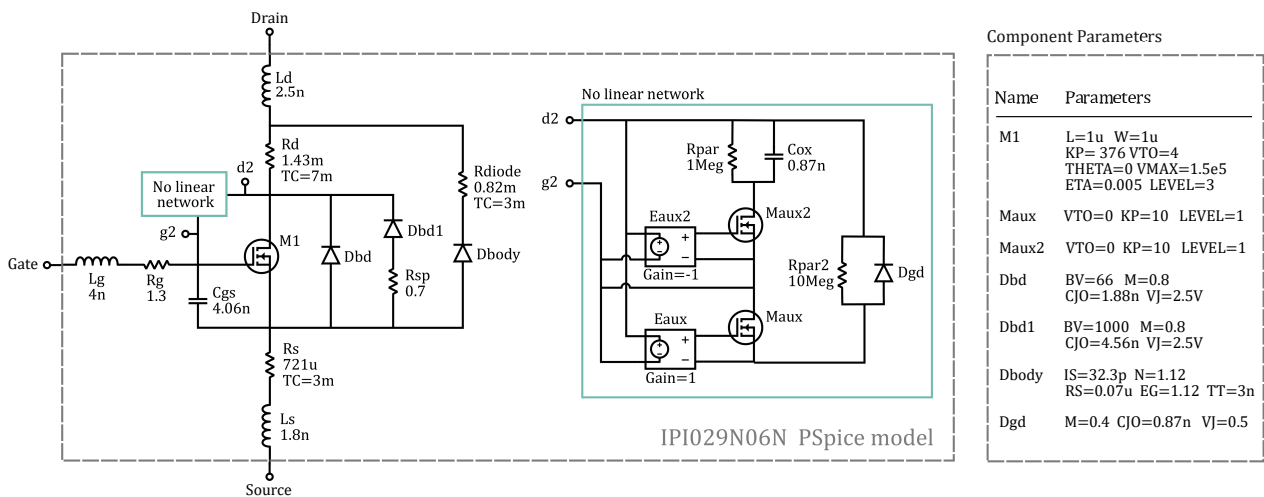


**Figure 6.** PSpice model of the IPI029N06N MOSFET used in simulations [40].

The three tuning methods were used in the design process to achieve soft-switching operation (i.e.,  $V_{SWon} = 0 \pm 10$  mV and  $\frac{dv_{SW}}{dt} = 0 \pm 0.1 \frac{V}{\mu s}$ , which was estimated by  $\frac{dv_{SW}}{dt} \approx \frac{I_{C_{SHon}}}{C_{SH}}$ ). The process results are illustrated in Figures 7–14, which summarize the initial and the final waveforms of each case study. Furthermore, the variables involved in this process are detailed in Tables 4–6. For the sake of clarity, the resulting component values (i.e., the selected values of the last sweep on each case study) are rewritten in Table 7. Using these values, the FoMs of the resulting amplifiers were calculated from the simulation results, and they are summarized in Table 8.

The case studies that achieved the two soft-switching conditions (i.e., ZVS and ZVDS) presented the expected nominal waveforms. For instance, in the  $C_{SH}$  sweep of case study 7, the ZVP values increased as  $C_{SH}$  increased, as shown in Figure 15a. However, case study 3 showed a non-expected tuning behavior during the component variations. As shown in Figure 15b, at the beginning of the  $C_{SH}$  tuning, the ZVP decreased (as we expected), and at the end this voltage increased. This unexpected inflection point made it difficult to achieve the ZVS and ZVDS, and limited the tuning process. Furthermore, this behavior was presented in other tuning process, and we refer to as the turning point in this paper. In particular, this unexpected behavior characterized the three tuning methods analyzed in case study 3; consequently, the number of parametric sweeps increased and ZVDS was not reached with tuning method 2, and the frequency value increased 299.8% concerning its initial value with tuning method 3. This case study is characterized by a  $Q_L$  value of 0.38 (i.e., a very low value); therefore, even in the ideal simulation,  $V_{SWon}$  and  $I_{C_{SHon}}$  were distant from zero because the assumptions of the ideal PA model were not met.

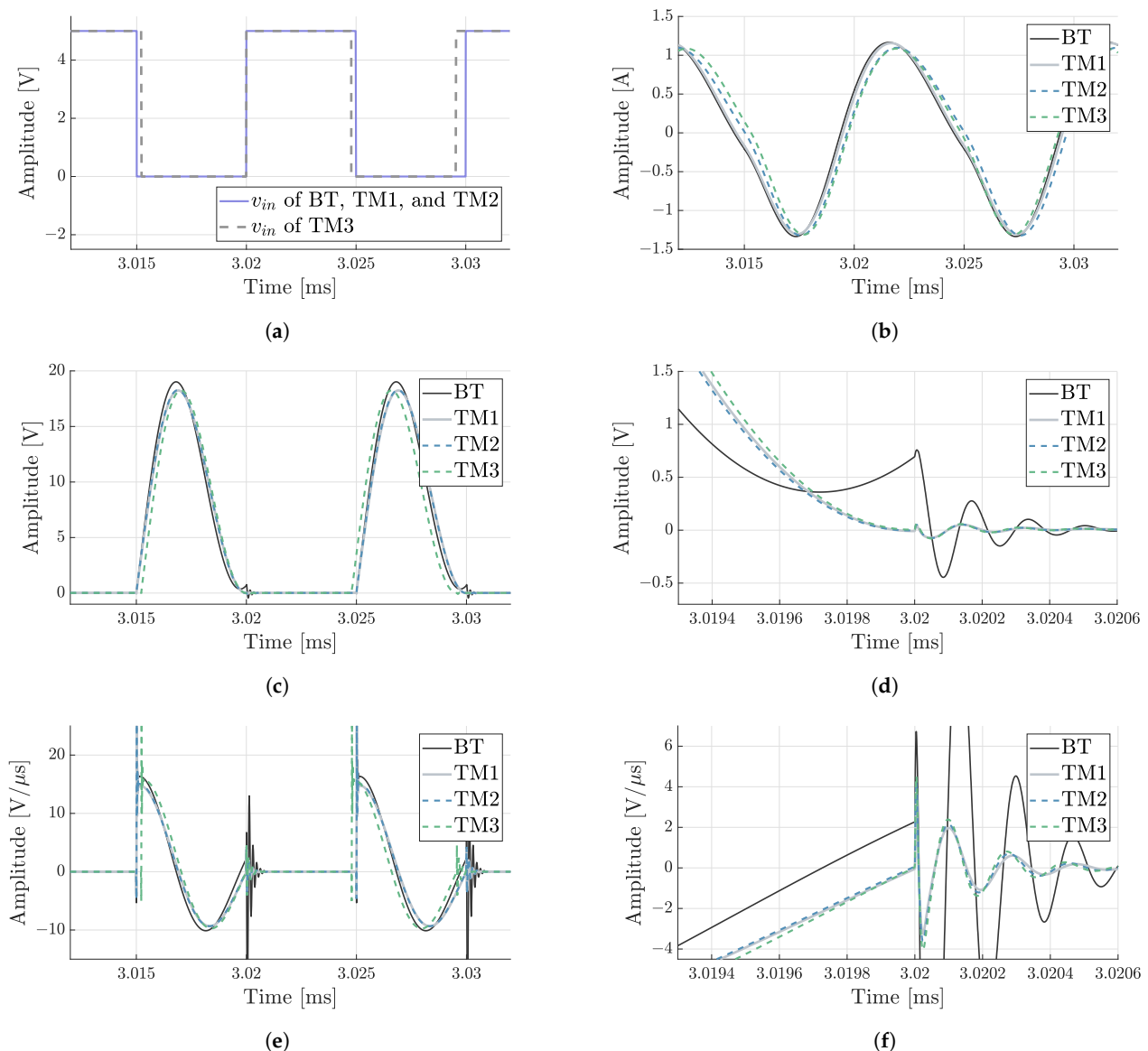


**Figure 7.** Waveforms before and after tuning of case study 1, where BT is the result before tuning. (a)  $v_{in}$ . (b)  $i_{RL}$ . (c)  $V_{SW}$ . (d)  $V_{SWon}$ . (e)  $\frac{dv_{SW}}{dt}$ . (f)  $\frac{dv_{SW}}{dt}$  at the switch turn-on time.

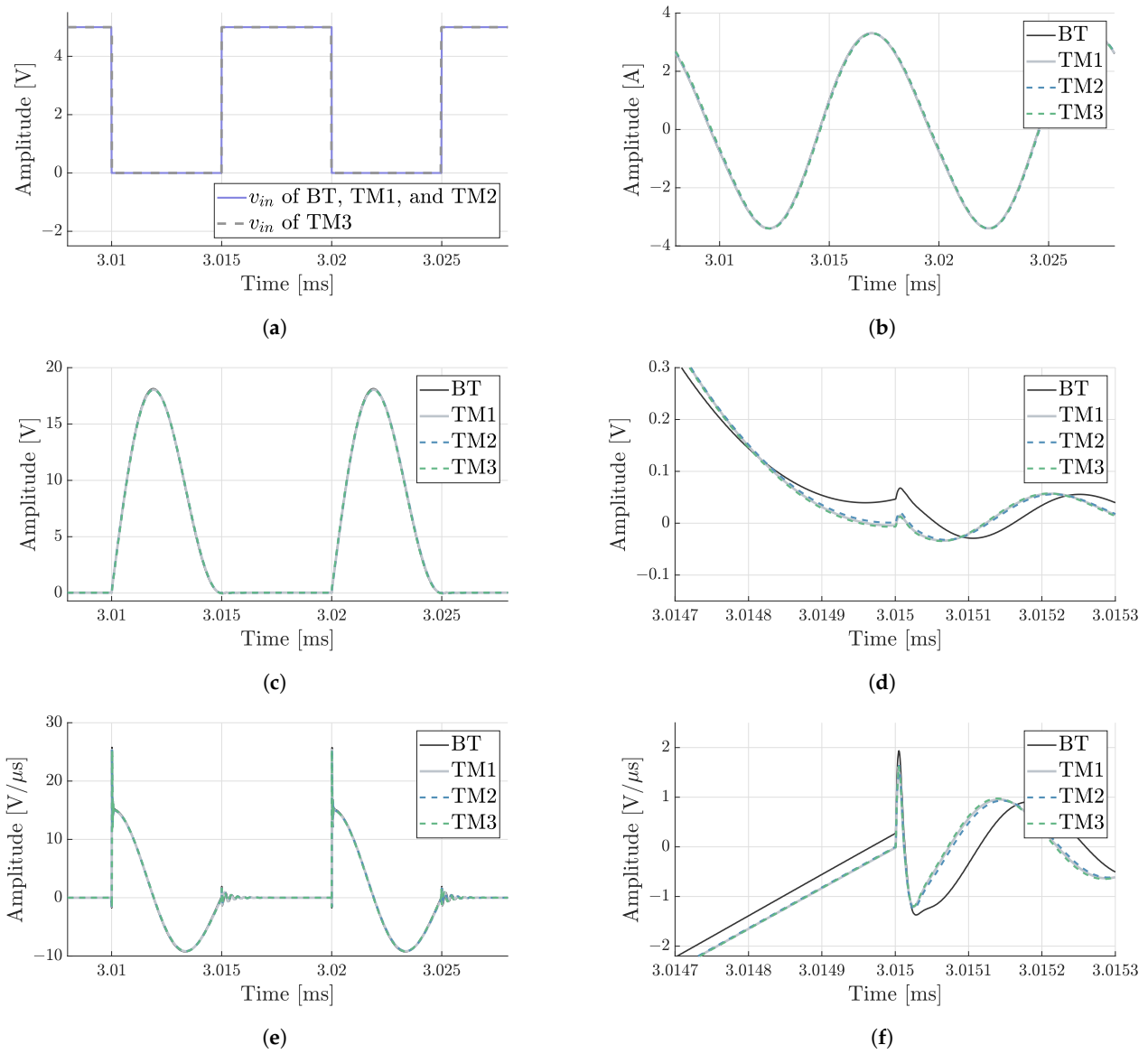


**Figure 8.** Waveforms before and after tuning of case study 2. (a)  $v_{in}$ . (b)  $i_{R_L}$ . (c)  $V_{SW}$ . (d)  $V_{SWon}$ . (e)  $\frac{dv_{SW}}{dt}$ . (f)  $\frac{dv_{SWon}}{dt}$  at the switch turn-on time.

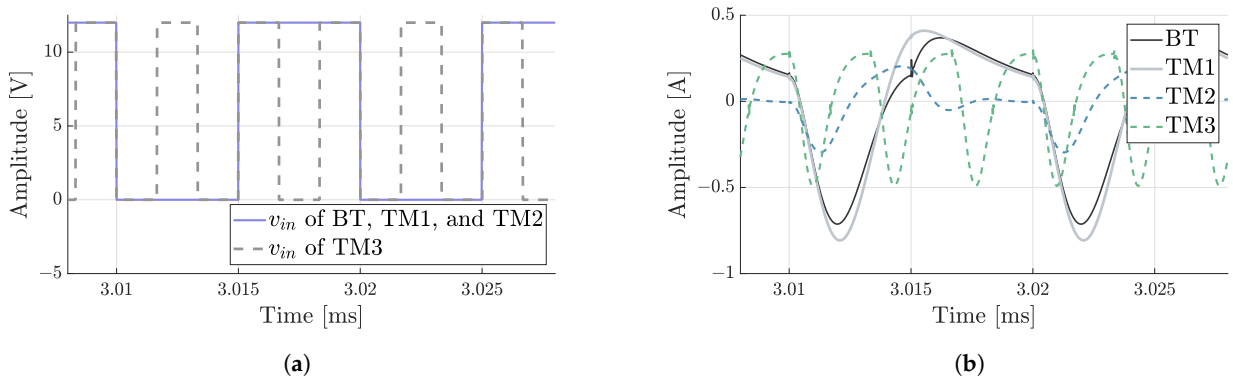


**Figure 9.** Cont.

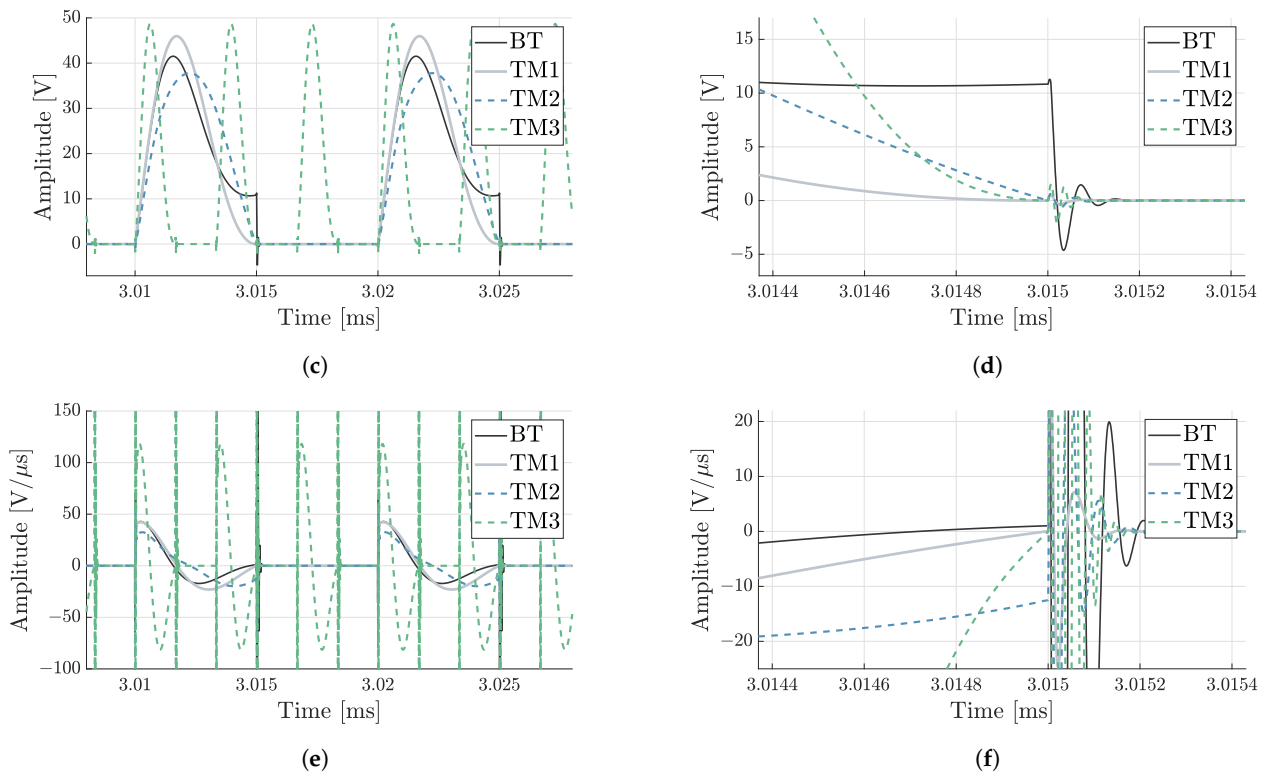


**Figure 9.** Waveforms before and after tuning of case study 3. (a)  $v_{in}$ . (b)  $i_{RL}$ . (c)  $V_{SW}$ . (d)  $V_{SWon}$ . (e)  $\frac{dv_{SW}}{dt}$ . (f)  $\frac{dv_{SW}}{dt}$  at the switch turn-on time.

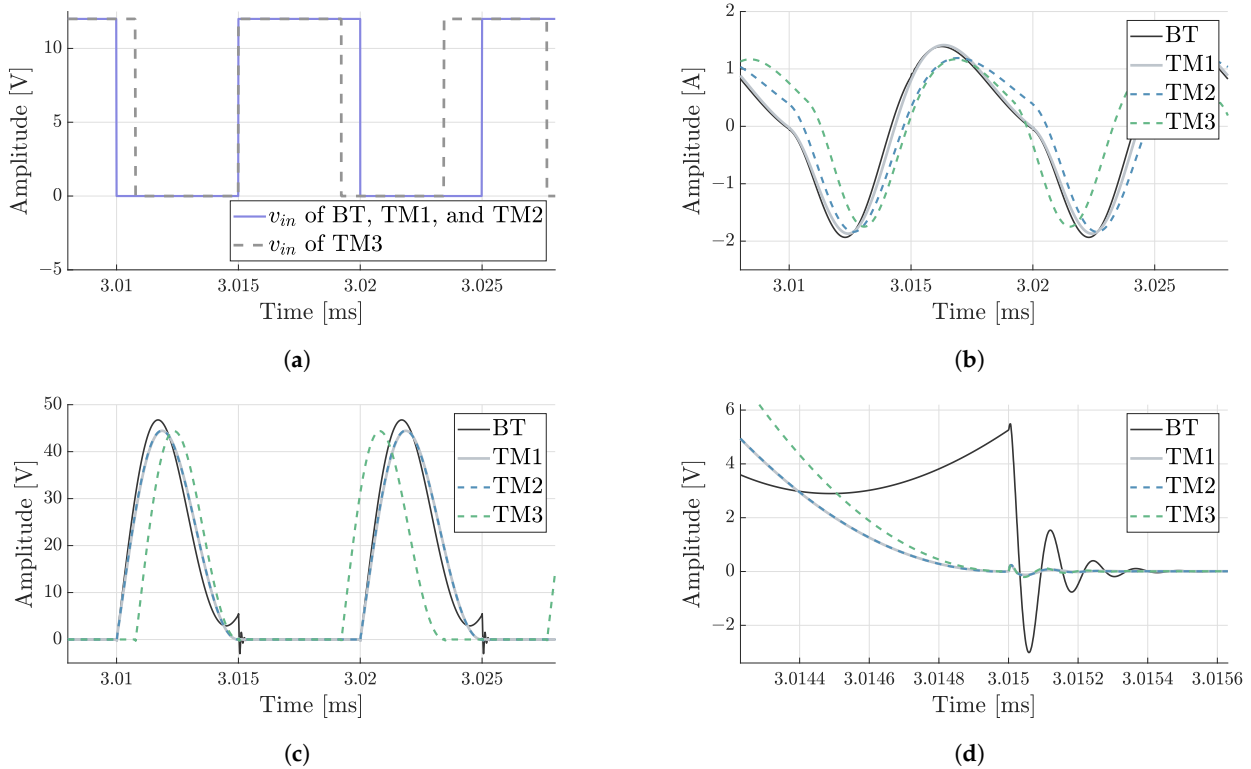


**Figure 10.** Cont.

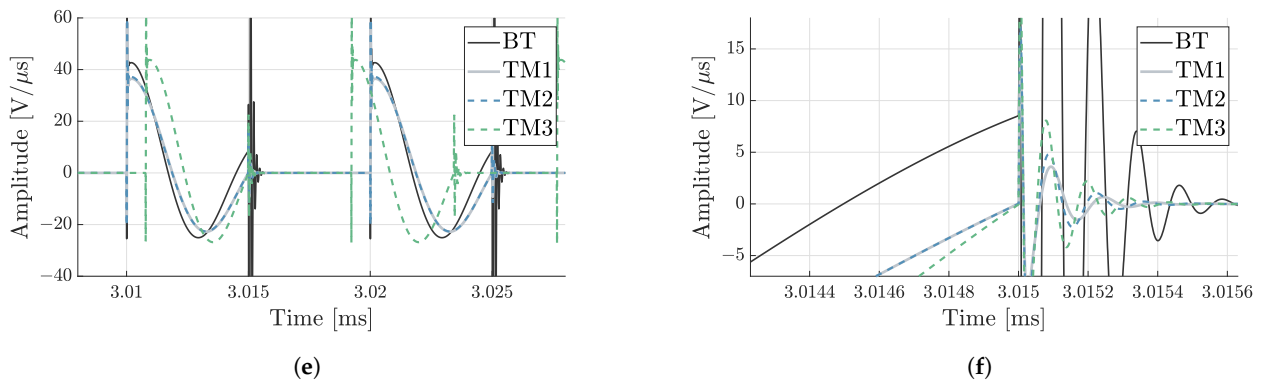


**Figure 10.** Waveforms before and after tuning of case study 4. (a)  $v_{in}$ . (b)  $i_{R_L}$ . (c)  $V_{SW}$ . (d)  $V_{SWon}$ . (e)  $\frac{dv_{SW}}{dt}$ . (f)  $\frac{dv_{SW}}{dt}$  at the switch turn-on time.

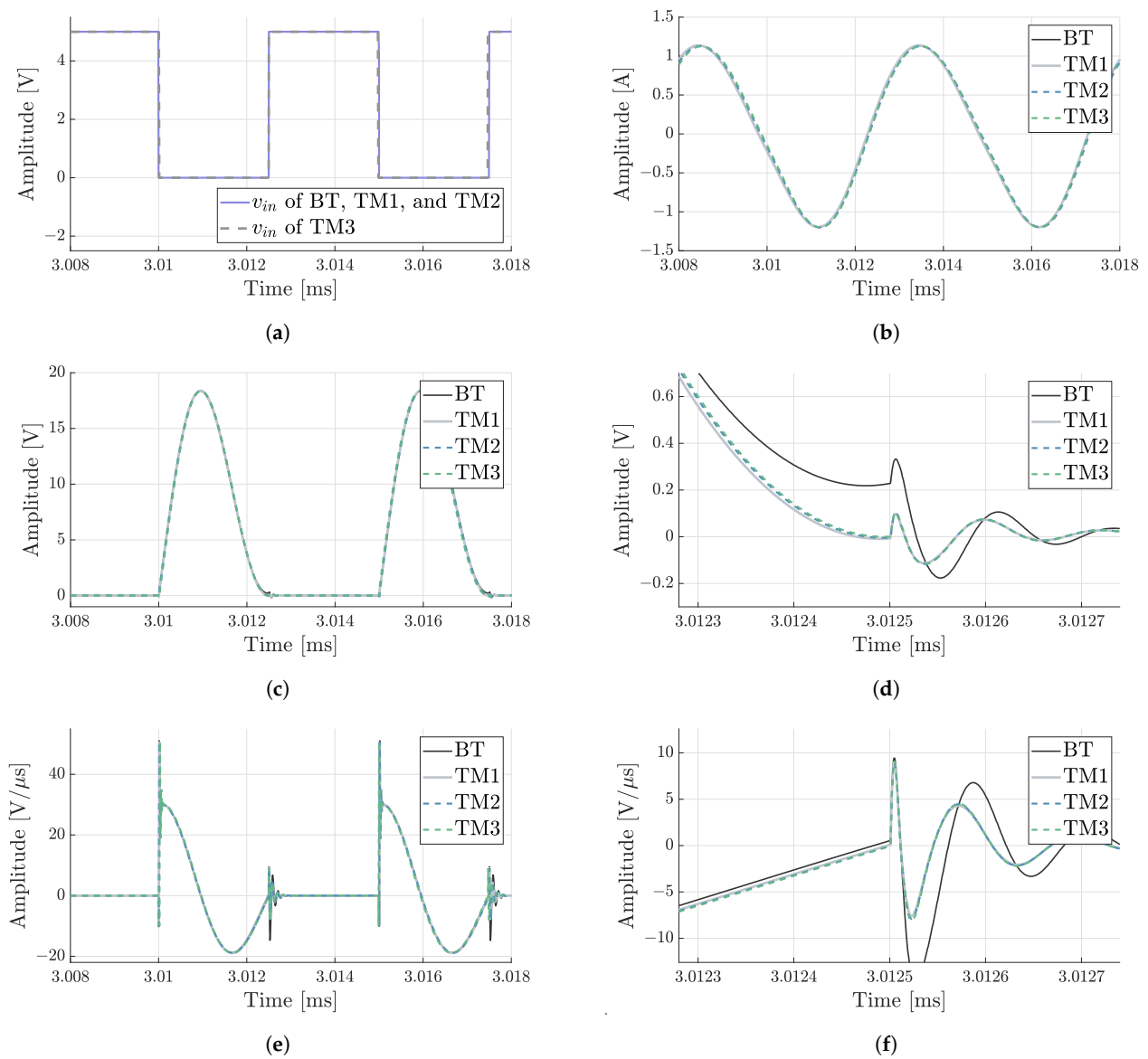


**Figure 11.** Waveforms before and after tuning of case study 5. (a)  $v_{in}$ . (b)  $i_{R_L}$ . (c)  $V_{SW}$ . (d)  $V_{SWon}$ . (e)  $\frac{dv_{SW}}{dt}$ . (f)  $\frac{dv_{SW}}{dt}$  at the switch turn-on time.

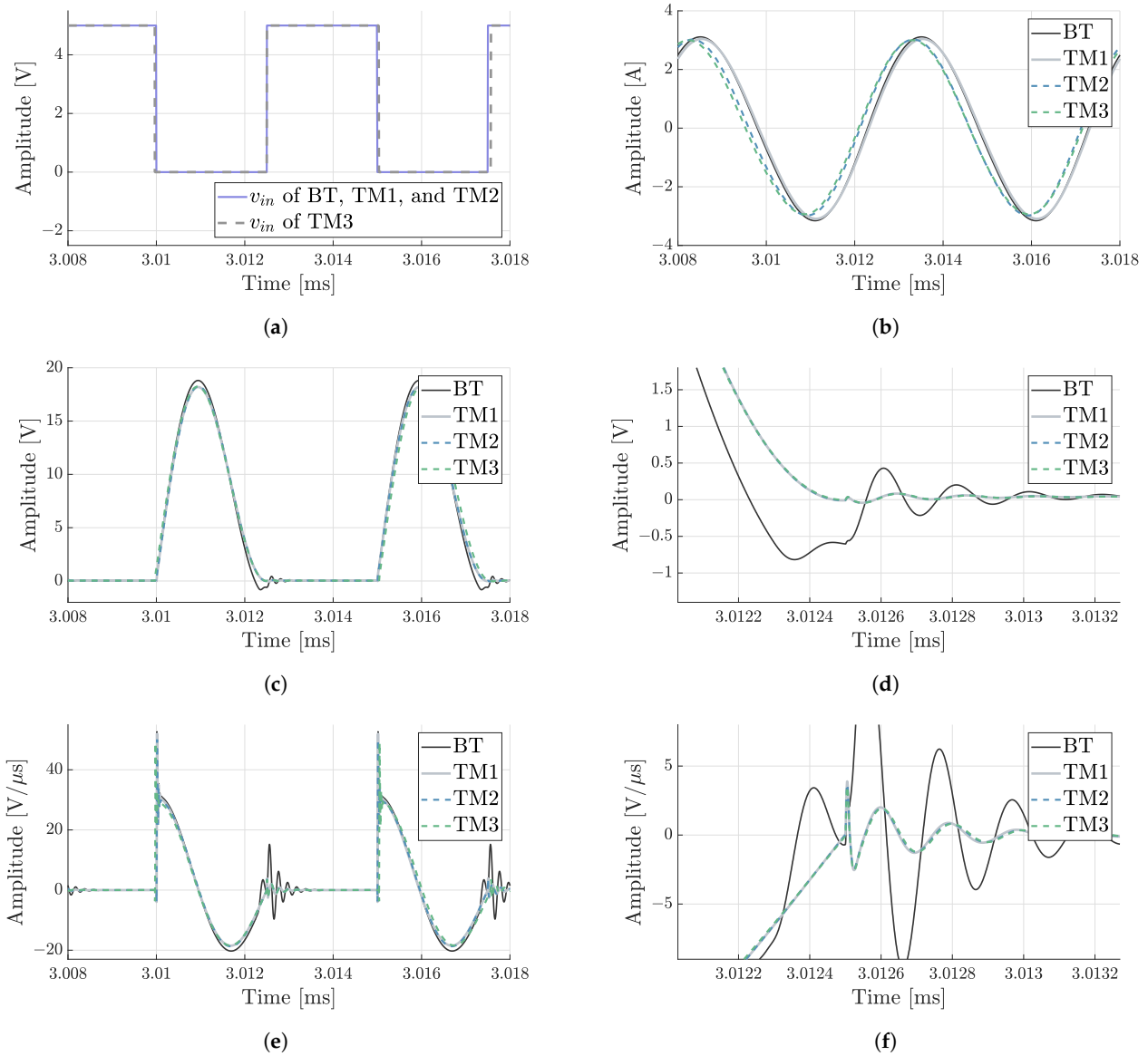


**Figure 12.** Waveforms before and after tuning of case study 6. (a)  $v_{in}$ . (b)  $i_{R_L}$ . (c)  $V_{SW}$ . (d)  $V_{SWon}$ . (e)  $\frac{dv_{SW}}{dt}$ . (f)  $\frac{dv_{SWon}}{dt}$  at the switch turn-on time.

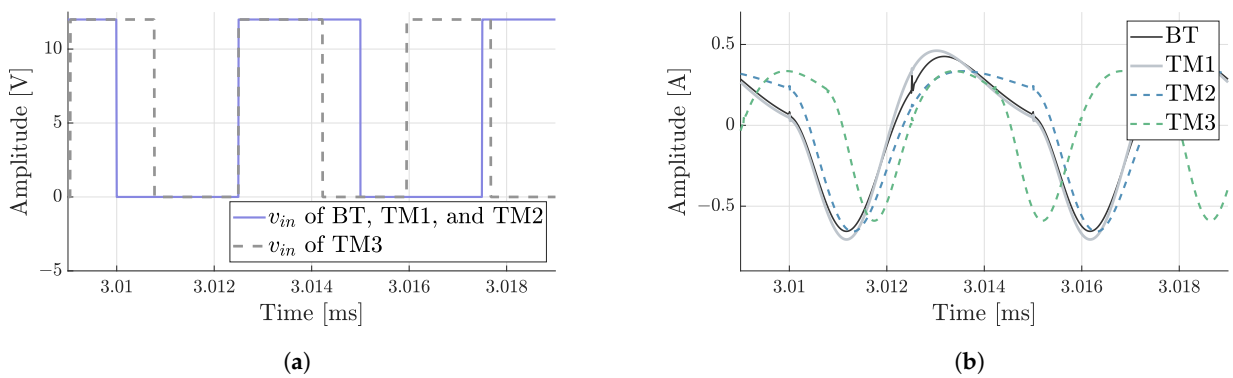


**Figure 13.** Cont.

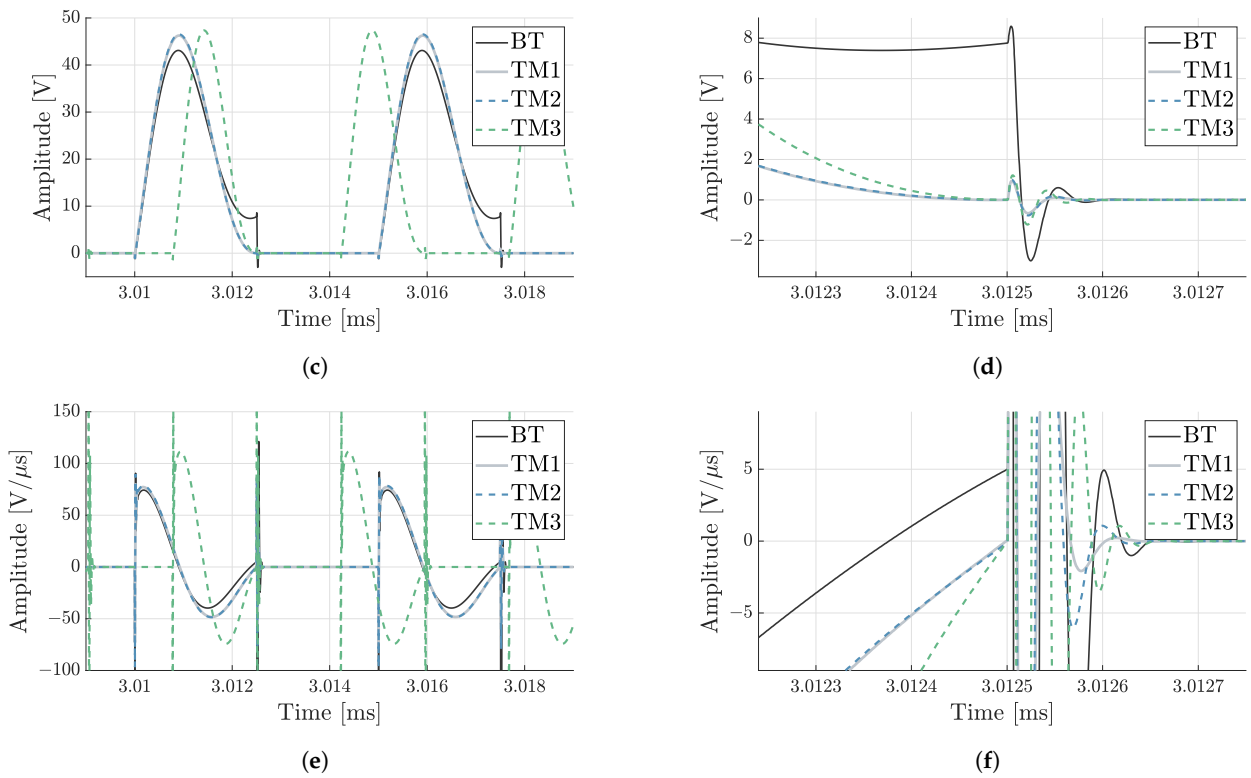


**Figure 13.** Waveforms before and after tuning of case study 7. (a)  $v_{in}$ . (b)  $i_{R_L}$ . (c)  $V_{SW}$ . (d)  $V_{SWon}$ . (e)  $\frac{dv_{SW}}{dt}$ . (f)  $\frac{dv_{SW}}{dt}$  at the switch turn-on time.

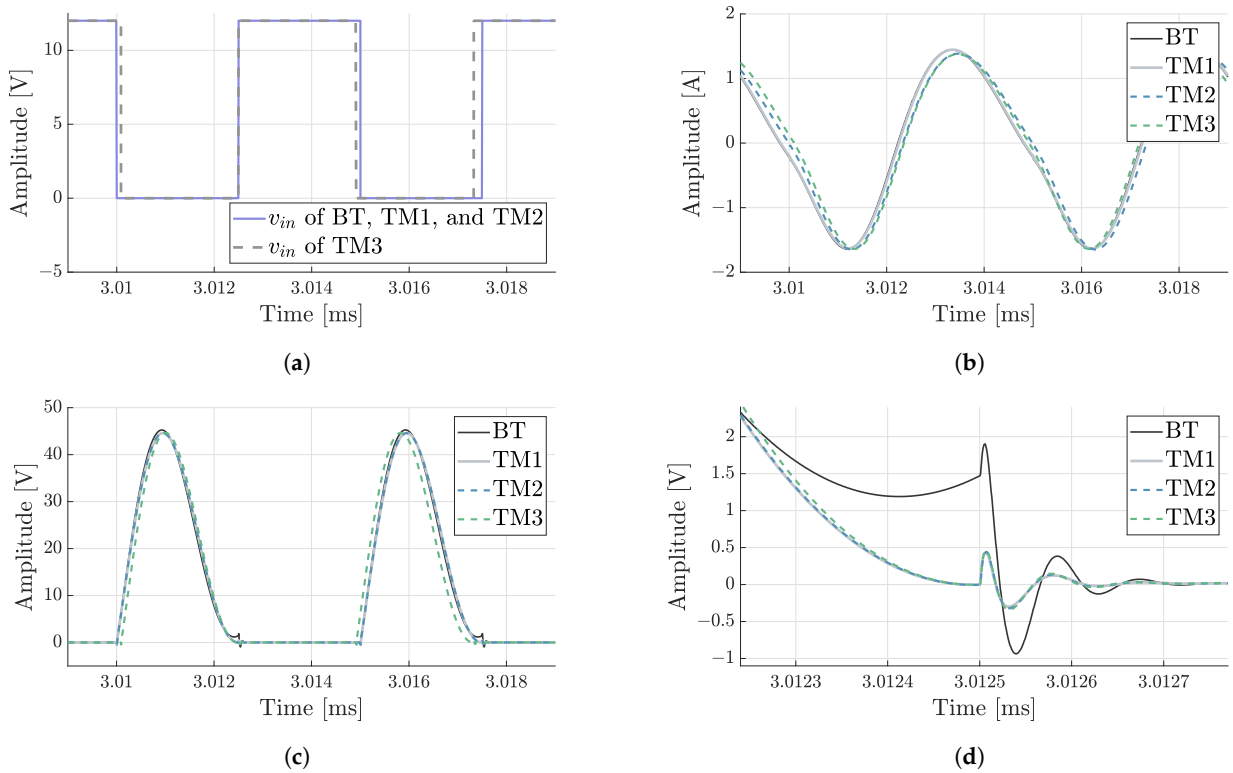


**Figure 14.** Cont.

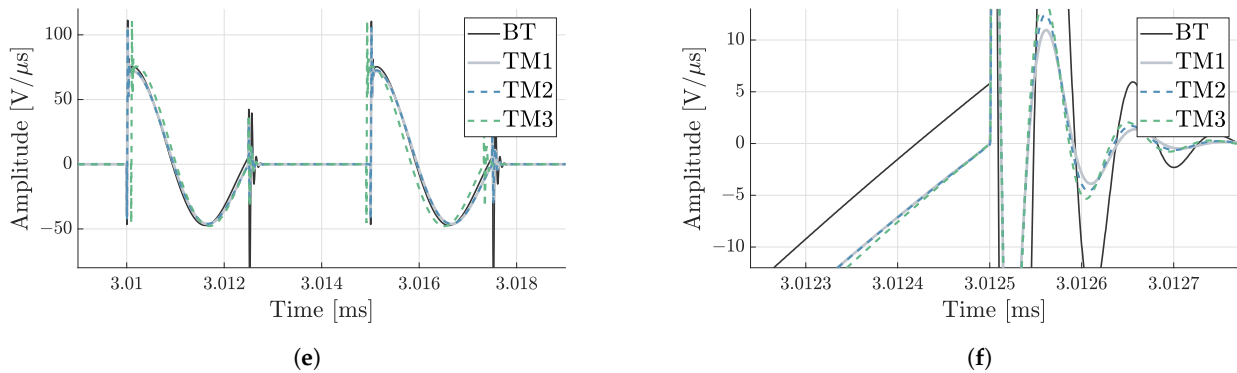


**Figure 14.** Waveforms before and after tuning of case study 8. (a)  $v_{in}$ . (b)  $i_{RL}$ . (c)  $V_{SW}$ . (d)  $V_{SWon}$ . (e)  $\frac{dv_{SW}}{dt}$ . (f)  $\frac{dv_{SW}}{dt}$  at the switch turn-on time.

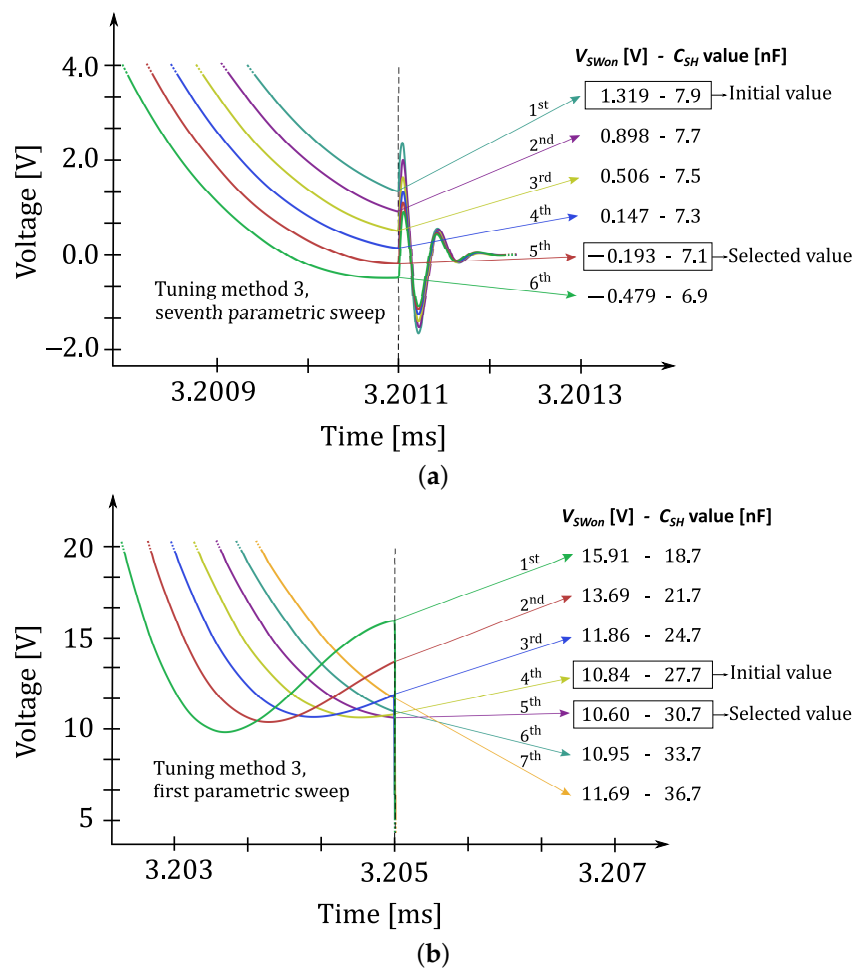


**Figure 15.**  $V_{SWon}$  responses to  $C_{SH}$  variations. (a) Expected  $V_{SWon}$  behavior in case study 7. (b) Unexpected turning point effect on  $V_{SWon}$  in case study 3.

Table 4. Parametric sweep values of the case studies using tuning method 1.

Case Study	Sweep Number	Component	Initial Value	Final Value	Increment Steps	Selected Value	$I_{C_{SHon}}$ [mA]	$V_{SWon}$ [mV]	$\frac{dv_{sw}}{dt}$ [V/ $\mu$ s]
1	1	$C_{SH}$ [nF]	159.7	184.7	5.0	184.7	−95.20	1722	−0.515
	2	$L_{SH}$ [ $\mu$ H]	6.500	8.000	0.30	7.100	146.9	74.80	0.795
	3	$C_{SH}$ [nF]	179.7	199.7	5.0	194.7	−45.82	550.6	−0.235
	4	$L_{SH}$ [ $\mu$ H]	5.600	7.100	0.30	6.800	58.51	−79.81	0.300
	5	$C_{SH}$ [nF]	194.7	199.7	1.0	199.7	−38.97	168.9	−0.195
	6	$L_{SH}$ [ $\mu$ H]	6.600	6.800	0.040	6.720	−9.754	−8.062 **	−0.0488
2	1	$L_{SH}$ [ $\mu$ H]	2.600	2.700	0.020	2.640	270.2	−291.1	0.564
	2	$C_{SH}$ [nF]	479.2	499.2	4.0	491.2	39.41	−55.05	0.0802
	3	$C_{SH}$ [nF]	491.2	495.2	0.50	493.7	−6.986	−4.389	−0.0141
3 *	1	$L_{SH}$ [ $\mu$ H]	30.80	45.80	5.0	35.80	155.5	9206	5.61
	2	$C_{SH}$ [nF]	17.70	47.70	5.0	37.70	−47.00	6862	−1.25
	3	$L_{SH}$ [ $\mu$ H]	15.80	35.80	5.0	30.80	82.71	4134	2.19
	4	$C_{SH}$ [nF]	27.70	37.70	2.0	37.70	82.71	4134	2.19
	5	$C_{SH}$ [nF]	37.70	87.70	10	57.70	−441.7	10,085	−7.66
	6	$L_{SH}$ [ $\mu$ H]	10.80	30.80	5.0	25.80	−354.6	4719	−6.15
	7	$C_{SH}$ [nF]	27.70	57.70	5.0	52.70	−203.1	2774	−3.85
	8	$L_{SH}$ [ $\mu$ H]	15.80	25.80	2.0	23.80	−95.35	467.6	−1.81
	9	$C_{SH}$ [nF]	42.70	52.70	2.0	48.70	53.04	−355.7	1.09
	10	$L_{SH}$ [ $\mu$ H]	23.80	24.80	0.20	24.00	39.88	−171.5	0.819
	11	$C_{SH}$ [nF]	48.70	52.70	1.0	49.70	2.905	−7.497	0.0584
4	1	$C_{SH}$ [nF]	83.20	133.2	10	103.2	−112.1	6758	−1.09
	2	$L_{SH}$ [ $\mu$ H]	5.300	15.30	2.0	11.30	753.7	959.9	7.30
	3	$C_{SH}$ [nF]	103.2	153.2	10	123.2	−121.7	1051	−0.988
	4	$L_{SH}$ [ $\mu$ H]	10.30	11.30	0.20	10.90	16.46	−142.2	0.134
	5	$L_{SH}$ [ $\mu$ H]	10.90	11.00	0.020	10.96	−5.786	38.91	−0.0470
	6	$C_{SH}$ [nF]	122.2	123.2	0.20	123.0	3.881	5.310	0.0316
5	1	$L_{SH}$ [ $\mu$ H]	3.800	4.000	0.040	3.840	124.5	−351.9	1.56
	2	$C_{SH}$ [nF]	79.90	84.90	1.0	82.90	13.47	−29.27	0.162
	3	$C_{SH}$ [nF]	82.90	83.90	0.20	83.10	7.204	−6.784	0.0867
6	1	$L_{SH}$ [ $\mu$ H]	1.300	1.800	0.10	1.500	−782.1	949.4	−3.26
	2	$C_{SH}$ [nF]	209.6	239.6	6.0	209.6	177.7	−494.0	0.848
	3	$L_{SH}$ [ $\mu$ H]	1.500	1.600	0.020	1.540	44.95	−102.7	0.214
	4	$L_{SH}$ [ $\mu$ H]	1.540	1.560	0.0050	1.550	14.71	−7.804	0.0702
7	1	$C_{SH}$ [nF]	13.90	23.90	2.0	19.90	−221.2	12,564	−11.1
	2	$L_{SH}$ [ $\mu$ H]	12.90	22.90	2.0	12.90	141.0	−17.61	7.08
	3	$C_{SH}$ [nF]	19.90	29.90	2.0	21.90	37.57	−538.0	1.72
	4	$L_{SH}$ [ $\mu$ H]	12.90	14.90	0.40	14.50	−85.95	1240	−3.92
	5	$C_{SH}$ [nF]	19.90	21.90	0.40	21.10	−27.51	602.0	−1.30
	6	$L_{SH}$ [ $\mu$ H]	13.50	14.50	0.20	14.30	−11.49	216.1	−0.544
	7	$L_{SH}$ [ $\mu$ H]	14.10	14.30	0.040	14.22	−5.142	63.66	−0.244
	8	$C_{SH}$ [nF]	21.00	21.10	0.010	21.01	1.454	2.104	0.0692
8	1	$C_{SH}$ [nF]	41.60	51.60	2.0	47.60	−225.4	4136	−4.74
	2	$L_{SH}$ [ $\mu$ H]	6.600	7.600	0.20	6.600	97.32	−548.5	2.04
	3	$C_{SH}$ [nF]	47.60	49.60	0.50	49.10	−30.38	61.68	−0.619
	4	$L_{SH}$ [ $\mu$ H]	6.600	6.700	0.20	6.640	−47.31	265.8	−0.964
	5	$C_{SH}$ [nF]	47.10	49.10	0.40	48.70	−14.08	84.83	−0.289
	6	$L_{SH}$ [ $\mu$ H]	6.600	6.640	0.010	6.630	−9.978	35.50	−0.205
	7	$C_{SH}$ [nF]	48.60	48.70	0.020	48.62	−3.196	−2.516	−0.0657

\* Turning point effect presented. \*\* Values reported in green satisfy the established soft-switching tolerance margins.

Table 5. Parametric sweep values of the case studies using tuning method 2.

Case Study	Sweep Number	Component	Initial Value	Final Value	Increment Steps	Selected Value	$I_{C_{SHon}}$ [mA]	$V_{SWon}$ [mV]	$\frac{dv_{SW}}{dt}$ [V/ $\mu$ s]
1	1	$C_e$ [nF]	105.5	125.5	5.0	110.5	438.8	−126.9	2.75
	2	$C_{SH}$ [nF]	159.7	179.7	5.0	179.7	32.47	545.1	0.181
	3	$C_e$ [nF]	110.5	130.5	5.0	115.5	65.63	−352.9	0.365
	4	$C_{SH}$ [nF]	179.7	189.7	2.0	181.7	26.55	−250.8	0.146
	5	$C_e$ [nF]	113.0	115.5	0.30	114.2	20.21	−22.80	0.111
	6	$C_{SH}$ [nF]	181.7	182.7	0.20	182.1	12.13	−1.981 **	0.0666
2	1	$C_e$ [nF]	105.5	110.5	1.0	106.5	237.2	−531.2	0.495
	2	$C_{SH}$ [nF]	479.2	499.2	5.0	489.2	40.69	−332.1	0.0832
	3	$C_e$ [nF]	105.5	106.5	0.20	105.9	−13.76	17.21	−0.0281
	4	$C_{SH}$ [nF]	479.2	489.2	2.0	487.2	23.02	−23.52	0.0472
	5	$C_{SH}$ [nF]	487.2	489.2	0.40	488.4	1.423	1.001	0.00291
3 *	1	$C_e$ [nF]	105.5	155.5	10	155.5	67.16	9168	2.42
	2	$C_e$ [nF]	155.5	255.5	20	255.5	98.58	7620	3.56
	3	$C_{SH}$ [nF]	7.700	27.70	5.0	27.70	98.58	7620	3.56
	4	$C_{SH}$ [nF]	27.70	47.70	5.0	32.70	−13.34	7005	−0.408
	5	$C_e$ [nF]	255.5	305.5	10	305.5	−9.156	6542	−0.280
	6	$C_e$ [nF]	305.5	405.5	20	405.5	−4.277	5955	−0.131
	7	$C_{SH}$ [nF]	12.70	32.70	5.0	27.70	115.9	6670	4.18
	8	$C_e$ [nF]	205.5	1005.5	100	1005.5	132.6	5666	4.79
	9	$C_{SH}$ [nF]	7.700	47.70	10	37.70	−134.4	6137	−3.57
	10	$C_e$ [nF]	1000	10,000	2000	9000	−135.0	5532	−3.58
	11	$C_{SH}$ [nF]	17.70	37.70	5.0	32.70	7.946	4231	0.243
	12	$C_e$ [nF]	9000	20,000	2000	19,000	8.201	4188	0.251
	13	$C_{SH}$ [nF]	2.700	62.70	10	32.70	8.201	4188	0.251
	14	$C_e$ [nF]	5.000	105.0	20	5.000	−546.7	11,391	−16.7
	15	$C_{SH}$ [nF]	2.700	32.70	6.0	20.70	0.07338	−680.2	0.00354
	16	$C_e$ [nF]	5.000	20.00	3.0	8.000	−0.2824	−672.1	−0.0136
	17	$C_e$ [nF]	8.000	11.00	0.50	9.500	−250.9	−222.0	−12.1
	18	$C_e$ [nF]	9.500	10.00	0.10	9.700	−259.1	74.46	−12.5
	19	$C_e$ [nF]	9.600	9.700	0.010	9.650	−259.9	4.019	−12.6
4	1	$C_e$ [nF]	105.5	155.5	10	155.5	666.7	1279	8.01
	2	$C_{SH}$ [nF]	83.20	133.2	10	103.2	39.75	−564.4	0.385
	3	$C_e$ [nF]	145.5	155.5	2.0	145.5	−23.59	110.2	−0.229
	4	$C_{SH}$ [nF]	101.2	103.2	0.40	102.4	11.59	−47.92	0.113
	5	$C_{SH}$ [nF]	102.4	102.8	0.10	102.6	2.537	−6.104	0.0247
5	1	$C_e$ [nF]	26.40	27.40	0.20	26.60	59.78	−76.21	0.748
	2	$C_{SH}$ [nF]	79.90	80.90	0.20	80.90	24.56	34.97	0.304
	3	$C_e$ [nF]	26.60	27.60	0.20	26.80	38.76	−272.5	0.479
	4	$C_{SH}$ [nF]	80.90	83.90	0.60	81.50	17.67	−205.4	0.217
	5	$C_e$ [nF]	26.30	26.80	0.10	26.70	11.50	−51.23	0.141
	6	$C_{SH}$ [nF]	81.50	82.50	0.20	81.90	−3.041	−3.611	−0.0371
6	1	$C_e$ [nF]	24.40	26.40	0.40	25.60	−802.3	1436	−3.35
	2	$C_{SH}$ [nF]	199.6	239.6	10	219.6	−167.4	408.4	−0.762
	3	$C_e$ [nF]	25.60	26.10	0.10	25.80	71.93	−109.5	0.328
	4	$C_{SH}$ [nF]	219.6	224.6	1.0	220.6	34.41	−63.19	0.156
	5	$C_e$ [nF]	25.30	25.80	0.10	25.80	34.58	−63.42	0.157
	6	$C_e$ [nF]	25.75	25.80	0.010	25.78	10.06	−6.314	0.0456
7	1	$C_e$ [nF]	26.40	56.40	6.0	56.40	99.47	−15.81	7.16
	2	$C_{SH}$ [nF]	13.90	18.90	1.0	15.90	−24.45	1069	−1.54
	3	$C_e$ [nF]	56.40	106.4	10	66.40	−27.28	175.2	−1.72
	4	$C_{SH}$ [nF]	14.90	15.90	0.20	15.50	−2.17	−174.4	−0.140
	5	$C_e$ [nF]	61.40	66.40	1.0	64.40	−2.559	−14.40	−0.165
	6	$C_e$ [nF]	63.90	64.40	0.10	64.20	−1.334	3.690	−0.0861
8	1	$C_e$ [nF]	26.40	28.40	0.40	27.60	290.2	−217.0	6.98
	2	$C_{SH}$ [nF]	41.60	46.60	1.0	44.60	46.91	547.7	1.05
	3	$C_e$ [nF]	27.60	28.60	0.20	28.00	58.94	−144.6	1.32
	4	$C_{SH}$ [nF]	44.60	46.60	0.40	45.00	25.90	43.93	0.575
	5	$C_e$ [nF]	28.00	28.50	0.10	28.10	28.80	−132.1	0.640
	6	$C_{SH}$ [nF]	45.00	46.00	0.20	45.40	−2.779	51.46	−0.0612
	7	$C_e$ [nF]	28.10	28.20	0.020	28.14	−2.586	−11.54	−0.0569
	8	$C_{SH}$ [nF]	45.40	45.50	0.020	45.42	−2.967	−1.511	−0.0653

\* Turning point effect presented. \*\* Values reported in green satisfy the established soft-switching tolerance margins.

Table 6. Parametric sweep values of the case studies using tuning method 3.

Case Study	Sweep Number	Component	Initial Value	Final Value	Increment Steps	Selected Value	$I_{CSH_{on}}$ [mA]	$V_{SW_{on}}$ [mV]	$\frac{dv_{SW}}{dt}$ [V/ $\mu$ s]
1	1	$C_{SH}$ [nF]	159.7	184.7	5.0	179.7	-15.68	1474	-0.0873
	2	$T_{vin}$ [ $\mu$ s]	9.000	10.00	0.20	9.600	-162.8	696.6	-0.906
	3	$C_{SH}$ [nF]	160.7	184.7	4.0	168.7	35.62	67.55	0.211
	4	$T_{vin}$ [ $\mu$ s]	9.500	9.600	0.020	9.560	16.51	-28.56	0.098 **
	5	$C_{SH}$ [nF]	168.7	169.7	0.20	169.3	4.694	5.663	0.0277
2	1	$C_{SH}$ [nF]	479.2	499.2	5.0	483.2	56.96	126.0	0.118
	2	$T_{vin}$ [ $\mu$ s]	9.950	10.00	0.010	9.970	74.31	-168.0	0.154
	3	$C_{SH}$ [nF]	483.2	493.2	2.0	487.2	-0.07901	-85.42	-0.000162
	4	$T_{vin}$ [ $\mu$ s]	9.970	9.980	0.0020	9.978	-3.841	-6.140	-0.00788
3 *	1	$C_{SH}$ [nF]	18.70	36.70	3.0	30.70	-20.15	10,597	-0.656
	2	$T_{vin}$ [ $\mu$ s]	8.000	10.00	0.40	8.400	-151.4	12,636	-4.93
	3	$C_{SH}$ [nF]	20.70	30.70	2.0	24.70	-13.05	10,658	-0.528
	4	$T_{vin}$ [ $\mu$ s]	7.400	8.400	0.20	7.400	-120.9	11,843	-4.90
	5	$C_{SH}$ [nF]	14.70	24.70	2.0	20.70	-8.304	10,164	-0.401
	6	$T_{vin}$ [ $\mu$ s]	6.400	7.400	0.20	6.400	-145.2	11,806	-7.02
	7	$C_{SH}$ [nF]	10.70	20.70	2.0	14.70	64.95	8843	4.42
	8	$T_{vin}$ [ $\mu$ s]	5.400	6.400	0.20	5.600	-70.66	8835	-4.81
	9	$C_{SH}$ [nF]	4.700	14.70	2.0	6.700	179.7	19,664	26.8
	10	$T_{vin}$ [ $\mu$ s]	3.600	5.600	0.40	0.4000	-10.19	2902	-1.52
	11	$C_{SH}$ [nF]	1.700	6.700	1.0	3.700	151.1	6968	40.8
	12	$T_{vin}$ [ $\mu$ s]	3.000	4.000	0.20	3.400	22.78	-305.4	6.16
	13	$C_{SH}$ [nF]	3.700	4.200	0.10	4.200	2.630	151.3	0.626
	14	$T_{vin}$ [ $\mu$ s]	3.300	3.400	0.020	3.340	-8.324	345.7	-1.98
	15	$C_{SH}$ [nF]	4.000	4.200	0.040	4.000	-1.712	-59.64	-0.428
	16	$T_{vin}$ [ $\mu$ s]	3.300	3.340	0.010	3.330	-1.103	-17.28	-0.276
	17	$C_{SH}$ [nF]	4.000	4.100	0.020	4.020	-0.9589	24.56	-0.239
	18	$T_{vin}$ [ $\mu$ s]	3.330	3.340	0.0020	3.336	0.01198	5.686	0.00298
4 *	1	$C_{SH}$ [nF]	83.20	133.2	10	103.2	-112.4	6758	-1.09
	2	$T_{vin}$ [ $\mu$ s]	7.500	10.00	0.50	9.000	-629.9	7077	-6.10
	3	$C_{SH}$ [nF]	73.20	103.2	10	83.20	120.7	2189	1.45
	4	$T_{vin}$ [ $\mu$ s]	7.000	9.000	0.50	8.500	-257.4	1800	-3.09
	5	$C_{SH}$ [nF]	63.20	83.20	5.0	78.20	-20.17	396.8	-0.258
	6	$T_{vin}$ [ $\mu$ s]	7.500	9.000	0.30	8.400	-104.0	341.5	-1.33
	7	$C_{SH}$ [nF]	75.20	78.20	0.50	75.70	21.47	-339.2	0.284
	8	$T_{vin}$ [ $\mu$ s]	8.400	8.60	0.040	8.440	55.60	-297.8	0.734
	9	$C_{SH}$ [nF]	75.70	77.70	0.50	76.70	2.721	-45.05	0.0355
	10	$C_{SH}$ [nF]	76.70	76.90	0.040	76.86	-3.805	-0.3965	-0.0495
5	1	$C_{SH}$ [nF]	79.90	82.90	0.50	81.90	-24.83	455.9	-0.303
	2	$T_{vin}$ [ $\mu$ s]	4.900	5.000	0.020	4.980	-28.01	223.8	-0.342
	3	$C_{SH}$ [nF]	79.90	81.90	0.40	81.10	-1.083	131.4	-0.0133
	4	$T_{vin}$ [ $\mu$ s]	4.960	4.980	0.0040	4.968	-5.930	-13.34	-0.0731
	5	$T_{vin}$ [ $\mu$ s]	4.968	4.972	0.0010	4.969	-3.785	0.1491	-0.0467
6	1	$C_{SH}$ [nF]	239.6	259.6	5.0	244.6	383.9	-604.5	1.57
	2	$T_{vin}$ [ $\mu$ s]	5.000	5.100	0.020	5.080	-786.9	1236	-3.22
	3	$C_{SH}$ [nF]	214.6	244.6	6.0	220.6	65.00	26.66	0.295
	4	$T_{vin}$ [ $\mu$ s]	5.060	5.080	0.0020	5.070	0.06500	-140.8	0.000295
	5	$C_{SH}$ [nF]	220.6	225.6	1.0	223.6	-13.26	-1.022	-0.0593
7 *	1	$C_{SH}$ [nF]	13.90	15.90	0.50	15.40	-16.18	8394	-1.05
	2	$T_{vin}$ [ $\mu$ s]	4.000	5.000	0.20	5.000	-16.18	8394	-1.05
	3	$T_{vin}$ [ $\mu$ s]	5.000	6.000	0.20	5.000	-16.18	8394	-1.05
	4	$C_{SH}$ [nF]	3.900	13.90	2.0	7.900	268.1	21,634	33.9
	5	$T_{vin}$ [ $\mu$ s]	4.000	5.000	0.20	4.000	174.6	2896	22.1
	6	$T_{vin}$ [ $\mu$ s]	3.400	4.000	0.20	3.400	-65.74	1319	-8.32
	7	$C_{SH}$ [nF]	6.900	7.900	0.20	7.100	-5.317	-192.8	-0.749
	8	$T_{vin}$ [ $\mu$ s]	3.400	3.450	0.010	3.450	11.45	-258.0	1.61
	9	$C_{SH}$ [nF]	7.100	7.310	0.050	7.260	-5.156	-40.65	-0.710
	10	$C_{SH}$ [nF]	7.260	7.310	0.010	7.280	0.2670	7.048	0.0367
8	1	$C_{SH}$ [nF]	41.60	51.60	2.0	43.60	73.49	2253	1.69
	2	$T_{vin}$ [ $\mu$ s]	4.000	5.000	0.20	4.800	-104.6	231.3	-2.40
	3	$C_{SH}$ [nF]	43.00	43.60	0.10	43.50	-96.34	178.4	-2.21
	4	$T_{vin}$ [ $\mu$ s]	4.600	4.800	0.040	4.780	-121.9	-20.20	-2.80
	5	$C_{SH}$ [nF]	43.50	43.70	0.050	43.55	-124.1	1.804	-2.85
	6	$T_{vin}$ [ $\mu$ s]	4.780	4.880	0.020	4.820	-78.99	406.6	-1.81
	7	$C_{SH}$ [nF]	42.55	43.55	0.20	42.75	-13.84	5.197	-0.324
	8	$C_{SH}$ [nF]	42.55	42.75	0.040	42.63	1.167	-60.62	0.0274
	9	$T_{vin}$ [ $\mu$ s]	4.820	4.830	0.0050	4.825	1.203	2.651	0.0282

\* Turning point effect presented. \*\* Values reported in green satisfy the established soft-switching tolerance margins.

**Table 7.** Component values of the class-E PA after the component tuning.

Case Study	Tuning Method	$L_{SH}$ [uH]	$C_{SH}$ [nF]	$C_e$ [nF]	$T_{v_{in}}$ [μs]
1	TM1	6.720	199.7	105.5	10.00
	TM2	8.000	182.1	114.2	10.00
	TM3	8.000	169.3	105.5	9.560
2	TM1	2.640	493.7	105.5	10.00
	TM2	2.700	488.4	105.9	10.00
	TM3	2.700	487.2	105.5	9.978
3	TM1	24.00	49.70	105.5	10.00
	TM2	Tuning does not converge			
	TM3	45.80	4.020	105.5	3.336
4	TM1	10.96	123.0	105.5	10.00
	TM2	15.30	102.6	145.5	10.00
	TM3	15.30	76.86	105.5	8.440
5	TM1	3.840	83.10	26.40	5.000
	TM2	4.000	81.90	26.70	5.000
	TM3	4.000	81.10	26.40	4.969
6	TM1	1.550	209.6	26.40	5.000
	TM2	1.300	220.6	25.78	5.000
	TM3	1.300	223.6	26.40	5.070
7	TM1	14.22	21.01	26.40	5.000
	TM2	22.90	15.50	64.20	5.000
	TM3	22.90	7.280	26.40	3.450
8	TM1	6.630	48.62	26.40	5.000
	TM2	7.600	45.42	28.14	5.000
	TM3	7.600	42.63	26.40	4.825

**Table 8.** Figures of merit of the class-E PA before and after the tuning process.

Case Study	Simulation	Iter. *	$V_{SWon}$ [mV]	$\frac{dv_{SW}}{dt}$ [V/μs]	THD [%]	$C_p$ [mW/W]	PAE [%]	$\eta$ [%]	$P_{VDD}$ [W]	$P_{out}$ [W]	
1	Ideal	0	434.1	3.01	17.28	0.9347	99.93	99.93	5.448	5.444	
	BT **	0	694.3	2.27	16.97	65.42	93.38	93.62	5.266	4.930	
	TM1	6	-8.062	-0.0488	16.05	68.41	92.41	92.64	5.200	4.817	
	TM2	6	-1.981	0.0666	15.95	69.91	93.26	93.50	5.022	4.696	
	TM3	5	5.663	0.0277	15.29	70.37	93.56	93.82	4.936	4.631	
2	Ideal	0	101.4	0.641	5.569	9.211	99.87	99.86	15.00	14.98	
	BT	0	46.65	0.273	5.857	85.48	89.50	89.59	14.23	12.75	
	TM1	3	-4.389	-0.0141	5.813	84.47	89.38	89.47	14.20	12.70	
	TM2	5	1.001	0.00291	5.808	84.91	89.48	89.57	14.17	12.69	
	TM3	4	-6.140	-0.00788	5.794	84.88	89.25	89.34	14.20	12.69	
3	Ideal	0	$11.35 \times 10^3$	2.31	46.60	0.03928	96.66	96.66	5.351	5.172	
	BT	0	$10.84 \times 10^3$	1.03	43.26	6.320	91.27	92.67	5.256	4.871	
	TM1	11	-7.497	0.0584	51.75	33.46	89.59	90.60	6.925	6.274	
	TM2				Tuning does not converge						
	TM3	20	5.686	0.00298	35.57	24.18	90.92	98.17	2.897	2.844	
4	Ideal	0	$5.180 \times 10^3$	11.0	31.15	0.1288	99.32	99.32	17.15	17.03	
	BT	0	$5.261 \times 10^3$	8.54	30.00	17.81	93.70	94.14	16.61	15.64	
	TM1	6	5.310	0.0316	28.24	52.38	92.11	92.52	16.88	15.62	
	TM2	5	-6.104	0.0247	27.71	52.63	93.92	94.38	15.06	14.21	
	TM3	10	-0.3965	-0.0495	24.52	53.23	94.51	95.10	14.04	13.35	

Table 8. Cont.

Case Study	Simulation	Iter. *	$V_{SWon}$ [mV]	$\frac{dv_{SW}}{dt}$ [V/ $\mu$ s]	THD [%]	$C_p$ [mW/W]	PAE [%]	$\eta$ [%]	$P_{VDD}$ [W]	$P_{out}$ [W]
5	Ideal	0	-29.68	2.91	8.495	18.96	99.95	99.95	5.215	5.213
	BT	0	230.8	0.543	8.390	71.78	90.85	91.34	4.901	4.477
	TM1	3	-6.784	0.0867	8.431	70.31	90.64	91.12	4.941	4.503
	TM2	6	-3.611	-0.0371	8.391	70.65	90.76	91.25	4.906	4.477
	TM3	5	0.1491	-0.0467	8.338	70.73	90.64	91.14	4.906	4.471
6	Ideal	0	-557.3	1.36	2.894	1.924	99.81	99.81	15.39	15.36
	BT	0	-604.2	-0.679	3.335	70.00	81.68	81.86	13.70	11.21
	TM1	4	-7.804	0.0702	3.147	78.99	82.80	82.99	12.94	10.74
	TM2	6	-6.314	0.0456	3.247	74.96	82.33	82.52	12.51	10.32
	TM3	5	-1.022	-0.0593	3.323	74.15	82.13	82.32	12.29	10.11
7	Ideal	0	$8.947 \times 10^3$	19.1	39.63	0.08600	98.03	98.03	5.689	5.577
	BT	0	$7.762 \times 10^3$	5.02	33.42	12.63	91.31	94.07	5.256	4.944
	TM1	8	2.104	0.0692	38.18	36.13	90.29	92.56	6.189	5.728
	TM2	6	3.690	-0.0861	37.90	33.84	92.15	94.93	5.030	4.775
	TM3	10	7.048	0.0367	30.92	32.72	91.77	96.49	4.296	4.146
8	Ideal	0	503.0	14.8	16.89	1.915	99.96	99.97	16.46	16.45
	BT	0	$1.470 \times 10^3$	5.81	15.83	59.95	92.86	93.77	15.50	14.54
	TM1	7	-2.516	-0.0657	15.58	57.10	92.11	93.01	15.62	14.53
	TM2	8	-1.511	-0.0653	15.46	57.63	92.60	93.51	15.19	14.21
	TM3	9	2.651	0.0282	14.96	57.90	92.59	93.55	15.07	14.10

\* Number of parametric sweeps to achieve a  $V_{SWon}$  between -10 and +10 mV and  $\frac{dv_{SW}}{dt}$  between -0.1 and +0.1 V/ $\mu$ s. \*\* BT = simulation before tuning, which was carried out using parasitic elements.

The tuning effect (TE) was quantified (only for the amplifiers with a successful tuning process) using the equations summarized in Table 9, based on simulation results before and after tuning (Table 8). Furthermore, the TE sign involves a positive or negative tuning impact on the related FoM. For instance, a positive value of the  $P_{out}$  TE involves an increase of the output power with a fixed input voltage, which is a positive tuning impact for an amplifier embedded in a wireless power transfer system.

Table 9. Tuning effects on the main figures of merit after the tuning process.

Case Study	Tuning Method	$TE_{C_p}^{**}$ [%]	$TE_{C_p}$ Sign	$TE_{THD}^*$ [%]	$TE_{THD}$ Sign	$TE_{P_{out}}^{**}$ [%]	$TE_{P_{out}}$ Sign	$TE_{\eta}^*$ [%]	$TE_{\eta}$ Sign	$TE_{PAE}^{**}$ [%]	$TE_{PAE}$ Sign
1	TM1	4.572	1	5.420	1	-2.282	-1	-1.044	-1	-1.046	-1
	TM2	6.872	1	6.004	1	-4.747	-1	-0.1207	-1	-0.1306	-1
	TM3	7.564	1	9.910	1	-6.069	-1	0.2147	1	0.1885	1
2	TM1	-1.185	-1	0.7478	1	-0.3374	-1	-0.1351	-1	-0.1363	-1
	TM2	-0.669	-1	0.8366	1	-0.4158	-1	-0.02679	-1	-0.02681	-1
	TM3	-0.704	-1	1.079	1	-0.4551	-1	-0.2813	-1	-0.2816	-1
3	TM1	429.4	1	-19.63	-1	28.82	1	-2.238	-1	-1.842	-1
	TM2	282.7	1	17.77	1	-41.60	-1	5.936	1	-0.3769	-1
4	TM1	194.1	1	5.877	1	-0.1407	-1	-1.712	-1	-1.698	-1
	TM2	195.5	1	7.647	1	-9.106	-1	0.2603	1	0.2305	1
	TM3	198.9	1	18.28	1	-14.61	-1	1.028	1	0.8687	1
5	TM1	-2.035	-1	-0.4863	-1	0.5853	1	-0.2398	-1	-0.2356	-1
	TM2	-1.562	-1	-0.01192	-1	0.002234	1	-0.1029	-1	-0.1024	-1
	TM3	-1.457	-1	0.6162	1	-0.1273	-1	-0.2222	-1	-0.2256	-1
6	TM1	12.84	1	5.629	1	-4.271	-1	1.379	1	1.367	1
	TM2	7.087	1	2.633	1	-7.954	-1	0.8112	1	0.7896	1
	TM3	5.930	1	0.3479	1	-9.818	-1	0.5705	1	0.5472	1
7	TM1	186.1	1	-14.25	-1	15.86	1	-1.611	-1	-1.117	-1
	TM2	168.0	1	-13.40	-1	-3.418	-1	0.9153	1	0.9122	1
	TM3	159.1	1	7.466	1	-16.15	-1	2.574	1	0.5038	1
8	TM1	-4.742	-1	1.579	1	-0.04128	-1	-0.8148	-1	-0.8066	-1
	TM2	-3.866	-1	2.356	1	-2.263	-1	-0.2719	-1	-0.2875	-1
	TM3	-3.415	-1	5.483	1	-3.034	-1	-0.2389	-1	-0.2972	-1

$$* TE = \frac{\text{FoM before tuning} - \text{FoM after tuning}}{\text{FoM before tuning}} \cdot 100; ** TE = \frac{\text{FoM after tuning} - \text{FoM before tuning}}{\text{FoM before tuning}} \cdot 100.$$

#### 4. Analysis of Results

The impacts of the tuning processes in the case studies were analyzed numerically based on the following statistics: the mean absolute percentage tuning effect (MAPTE), the TE factor and the standard deviations (Std Dev.). Furthermore, these statistics were calculated based on the TE values listed in Table 9. The MAPTE has been defined as the impact magnitude of the tuning process on the related FoM of the amplifier, which was calculated by the average value of the absolute values of the tuning effect. The TE factor has been defined as a normalized value between  $-1$  and  $1$ , which is related to the average impact of the tuning process on FoMs. On one hand, if all the FoMs were to be characterized by a positive tuning effect, the resulting TE factor would be  $+1$ . On the other hand, if the resulting factor were to be  $-1$ , the overall FoMs were characterized by a negative tuning effect. Furthermore, the resulting factor is  $0$  only when the numbers of FoMs characterized by positive and negative impacts are the same. This factor was calculated as follows: the sign function was applied to the TE value of each FoM (i.e., the sign function result is  $+1$ ,  $-1$  or  $0$  if TE value is positive, negative or zero, respectively); next, the average value was calculated. These values and the involved statistics were calculated for each tuning method, case study and FoM, as summarized in Tables 10–12, respectively.

The overall statistics related to each tuning method (summarized in Table 10) are very similar. Consequently, these statistics are not useful for discriminating the analyzed tuning methods. Furthermore, these methods were characterized by a negative impact on the FoMs in an average sense. However, this trend was not consistent for all of the case studies, because their standard deviations are higher than their mean values. Moreover, the analyzed tuning methods were successful (i.e., achieved quasi-soft-switching operation) in 95.8% of the analyzed amplifiers. Furthermore, they converged in few iterations (less than 10 in the 79.2% of cases). It is important to note that the number of iterations will depend on the established tolerance margins (i.e., less than 10 mV and  $0.1 \frac{V}{\mu s}$ ), the number of lines displayed in each parametric sweep and the designer experience. This number of iterations provides an estimation of the resources required in each method (e.g., computation time).

The tuning effect depends directly on the case study, as shown in the statistics summarized in Table 11. For instance, the highest MAPTE and a positive TE factor occurred in case studies 4 and 7, whereas case 8 has the biggest value of MAPTE related to a negative value of the TE factor. Therefore, the bigger and more positive impacts were present in the case studies where the supply voltage was higher. However, as an exception to this trend, case 8 was characterized by a big negative impact of the tuning process. Another trend is that the FoMs most affected by the tuning process were THD and  $C_p$ .

**Table 10.** Resulting statistics of the tuning effect grouped by method.

Tuning Method	Average Iterations	Unsuccessful Tuning [%]	MAPTE	Std Dev. MAPTE	TE Factor	Std Dev. TE Factor
TM1	6.00	0.00	23.96	78.69	$-0.2500$	0.9806
TM2	6.00	12.5	12.84	43.21	$-0.08571$	1.011
TM3	8.50	0.00	20.67	59.53	0.1000	1.008
Mean	6.83	4.17	19.16	60.48	$-0.07857$	1.000

The highest MAPTE and a positive TE factor of the statistical results listed in Table 12 occurred for  $C_p$  and THD, which were improved in 61% and 78% of the reported cases, respectively. Moreover, the PAE had the lowest MAPTE with a negative TE factor and was improved only in 35% of cases listed in Table 8. Accordingly, the nominal class-E operation does not guarantee the maximum efficiency of the amplifier; its optimal  $\eta$  and PAE are achieved under off-nominal class-E operation [31]. Finally, from the results it is clear that all the FoMs cannot be optimized simultaneously because of the trade-offs involved between the amplifier variables. Finally, Table 13 summarizes the TE factor statistics, which are grouped by tuning method and figures of merit. Contrary to TM1 and TM2, TM3 (i.e.,  $C_{SH}$  and  $T_{vin}$ )

had a positive impact and the highest TE factor for almost all the FoMs (i.e., without  $P_{out}$ ), in the average sense. Furthermore, in 100% of the case studies, TM3 increased and decreased the THD and the output power, respectively.

**Table 11.** Resulting statistics of the tuning effect grouped by case study.

Case Study	PA Specifications			MAPTE	Std. Dev. MAPTE	TE Factor	Std. Dev. TE Factor	TE	
	Freq. [kHz]	VDD [V]	Pout [W]					Best FoM	Worst FoM
3	100	12	5.0	83.03	155.9	0.0000	1.054	$C_p$	$P_{out}$
4	100	12	15	43.33	81.30	0.3333	0.976	$C_p$	$P_{out}$
7	200	12	5.0	39.42	72.22	0.2000	1.014	$C_p$	THD
6	200	5.0	15	4.132	5.677	0.6000	0.8281	$C_p$	$P_{out}$
1	100	5.0	5.0	3.746	4.729	0.0667	1.033	THD	$P_{out}$
8	200	12	15	1.966	2.613	−0.6000	0.8281	THD	$C_p$
2	100	5.0	15	0.4878	0.6092	−0.6000	0.8281	THD	$C_p$
5	200	5.0	5.0	0.5341	0.7474	−0.6000	0.8281	$P_{out}$	$C_p$

N.A.: not applicable; this value was not evaluated because tuning did not converge.

**Table 12.** Resulting statistics of the tuning effect grouped by FoM.

FoM	MAPTE	Std Dev. MAPTE	TE Factor	Std Dev. TE Factor
$C_p$	81.66	120.8	0.217	0.998
THD	6.411	8.772	0.565	0.843
PAE	0.6095	0.8003	−0.304	0.974
$\eta$	0.9890	1.630	−0.217	0.998
$P_{out}$	7.483	12.34	−0.652	0.775

**Table 13.** Resulting statistics of the TE factor grouped by tuning method and FoM.

Tuning Method	TE Factor THD	TE Factor $C_p$	TE Factor PAE	TE Factor $\eta$	TE Factor $P_{out}$
TM1	0.25	0.25	−0.75	−0.75	−0.25
TM2	0.43	0.14	−0.14	−0.14	−0.71
TM3	1.0	0.25	0.00	0.25	−1.0
Mean	0.56	0.21	−0.30	−0.21	−0.65

## 5. Conclusions

This paper explored a design methodology for a class-E amplifier with FDI, based on component tuning and oriented toward soft-switching operation. The results of eight case studies show that there are no direct relations between soft-switching operation and the optimum values of the amplifiers FoM, as is reported for conventional class-E amplifiers with choke. Furthermore, the improvement of the FoMs with the soft-switching tuning was effective only for a few case studies. The FoMs more affected by this tuning process were the total harmonic distortion and the output power capability, which were improved in 78% and 61% of cases. Moreover, in 79.2% of the case studies, the tuning process achieved soft-switching operation after few iterations. However, tuning method 3 (i.e.,  $C_{SH}$  and  $T_{v_{in}}$ ) had positive impacts on almost all the FoMs in the average sense. Furthermore, this method decreased the power output in 100% of the case studies, and increased the other FoMs in more case studies than tuning methods 1 and 2.

## 6. Future Work

This paper presents the results of one the first milestones reached under the framework of the research projects entitled “Class E Amplifier with Gallium Nitride Transistors for Wireless Power Transfer Applications” and “Class-E power amplifier as an electromagnetic interference source under soft and forced switching operation.” In future work, we will

evaluate the effects of the soft-switching tuning on other FoMs related to understanding the class-E PA as an EMI (electromagnetic interference) source. Furthermore, we will analyze the electromagnetic compatibility of a generic wireless power transfer (WPT) system with an embedded class-E amplifier. Additionally, we will explore non-soft-switching tuning methods to improve the figures of merit of a class-E PA with FDI embedded in a WTP system, which requires the simultaneous maximization of the power efficiency and output power.

**Author Contributions:** Conceptualization, I.C., C.-I.P.-R., G.P., M.P. and A.F.; methodology, I.C., C.-I.P.-R., G.P., M.P. and A.F.; software, C.-I.P.-R., I.C., R.U. and A.F.; validation, I.C., R.U., and A.F.; writing—original draft preparation, I.C., C.-I.P.-R., G.P., M.P. and A.F.; writing—review and editing, all authors; visualization, I.C., R.U. and A.F.; supervision, A.F., C.-I.P.-R., G.P. and M.P. All authors have read and agreed to the published version of the manuscript.

**Funding:** This research was funded by Pontificia Universidad Javeriana through two research projects, which were titled “Class E Amplifier with Gallium Nitride Transistors for Wireless Power Transfer Applications” and “Class-E power amplifier as an electromagnetic interference source under soft and forced switching operation.” They are identified with IDs 20066 and 09376, respectively. The APC was funded by the Pontificia Universidad Javeriana.

**Data Availability Statement:** The data presented in this study are available on request from the corresponding author.

**Acknowledgments:** This research was funded by Pontificia Universidad Javeriana through two research projects, which were titled “Class E Amplifier with Gallium Nitride Transistors for Wireless Power Transfer Applications” and “Class-E power amplifier as an electromagnetic interference source under soft and forced switching operation.” They are identified with IDs 20066 and 09376, respectively. The APC was funded by the Pontificia Universidad Javeriana. Additionally, the authors would like to thank the Electronics Department and Electronics laboratory of the Pontificia Universidad Javeriana, for providing the resources required to conduct this study.

**Conflicts of Interest:** The authors declare no conflict of interest.

### Abbreviations

The following abbreviations are used in this manuscript:

PA	Power Amplifier
RF	Radio-Frequency
ZVS	Zero Voltage Switching
ZVDS	Zero Voltage Derivative Switching
FDI	Finite DC-Feed Inductance
MAPTE	Mean Absolute Percentage Tuning Effect

### References

1. Abbas, S.M.; Hannan, M.A.; Salina, A.S. Efficient Class-E design for inductive powering wireless biotelemetry applications. In Proceedings of the 2012 International Conference on Biomedical Engineering (ICoBE), Penang, Malaysia, 27–28 February 2012; pp. 445–449. [\[CrossRef\]](#)
2. Peña-Eguiluz, R.; Pérez-Martínez, J.A.; López-Callejas, R.; Mercado-Cabrera, A.; Solís-Pacheco, J.; Aguilar-Uscanga, B.; Muñoz-Castro, A.E.; Valencia-Alvarado, R.; Barocio-Delgado, S.R.; Rodríguez-Méndez, B.G.; et al. Analysis and Application of a Parallel E-Class Amplifier as RF Plasma Source. *IEEE Trans. Plasma Sci.* **2010**, *38*, 2840–2847. [\[CrossRef\]](#)
3. Liu, S.; Liu, M.; Han, S.; Zhu, X.; Ma, C. Tunable Class  $E^2$  DC–DC Converter With High Efficiency and Stable Output Power for 6.78-MHz Wireless Power Transfer. *IEEE Trans. Power Electron.* **2018**, *33*, 6877–6886. [\[CrossRef\]](#)
4. Gurov, K.O. Study of a Class E Power Amplifier Tuning Effect on Output Power and Efficiency of an Inductive Wireless Power Transfer System. In Proceedings of the 2021 IEEE Conference of Russian Young Researchers in Electrical and Electronic Engineering (ElConRus), Moscow, Russia, 26–29 January 2021; pp. 2803–2807.
5. Qaragoz, Y.M.; Ali, I.; Kim, S.J.; Lee, K. A 5.8GHz 9.5 dBm Class-E Power Amplifier for DSRC Applications. In Proceedings of the 2019 International SoC Design Conference (ISOCC), Jeju, Korea, 6–9 October 2019; pp. 202–203.
6. Eroglu, A.; Sivakumar, S. Phase controlled Class E amplifiers for pulsing applications. In Proceedings of the 2009 IEEE MTT-S International Microwave Symposium Digest, Boston, MA, USA, 7–12 June 2009; pp. 765–768. [\[CrossRef\]](#)

7. Gorain, C.; Sadhu, P.K.; Raman, R. Analysis of High-Frequency Class E Resonant Inverter and its Application in an Induction Heater. In Proceedings of the 2018 2nd International Conference on Power, Energy and Environment: Towards Smart Technology (ICEPE), Shillong, India, 1–2 June 2018; pp. 1–6.
8. Mangkalajan, S.; Ekkaravarodome, C.; Jirasereamornkul, K.; Thounthong, P.; Higuchi, K.; Kazimierzczuk, M.K. A Single-Stage LED Driver Based on ZCDS Class-E Current-Driven Rectifier as a PFC for Street-Lighting Applications. *IEEE Trans. Power Electron.* **2018**, *33*, 8710–8727. [[CrossRef](#)]
9. Kessler, D.J.; Kazimierzczuk, M.K. Power losses and efficiency of class-E power amplifier at any duty ratio. *IEEE Trans. Circuits Syst. I Reg. Papers* **2004**, *51*, 1675–1689. [[CrossRef](#)]
10. Sokal, N.O.; Sokal, A.D. Class E-A new class of high-efficiency tuned single-ended switching power amplifiers. *IEEE J. Solid State Circuits* **1975**, *10*, 168–176. [[CrossRef](#)]
11. Raab, F. Idealized operation of the class E tuned power amplifier. *IEEE Trans. Circuits Syst.* **1977**, *24*, 725–735. [[CrossRef](#)]
12. Casallas, I.; Páez, C.; Perilla, G.; Fajardo, A. Design methodology of Class-E power amplifier using feed inductance tuning for high-efficiency operation in wireless power transfer applications. In Proceedings of the ANDESCON 2020 Conference, Quito, Ecuador, 13–16 October 2020; pp. 869–874.
13. Zulinski, R.; Steadman, J. Class E Power Amplifiers and Frequency Multipliers with finite DC-Feed Inductance. *IEEE Trans. Circuits Syst.* **1987**, *34*, 1074–1087. [[CrossRef](#)]
14. Li, C.; Yam, Y. Maximum frequency and optimum performance of class E power amplifiers. *IEE. Proc. Circuits Devices Syst.* **1994**, *141*, 174–184. [[CrossRef](#)]
15. Choi, D.K.; Long, S.I. Finite DC feed inductor in class E power amplifiers—a simplified approach. In Proceedings of the IEEE International Microwave Symposium Digest, Seattle, WA, USA, 2–7 June 2002; Volume 3, pp. 1643–1646.
16. Sekiya, H.; Sasase, I.; Mori, S. Computation of design values for Class E amplifiers without using waveform equations. *IEEE Trans. Circuits Syst. I Fundam. Theory* **2002**, *49*, 966–978. [[CrossRef](#)]
17. Milosevic, D.; van der Tang, J.; van Roermund, A. Explicit design equations for class-E power amplifiers with small DC-feed inductance. In Proceedings of the 2005 European Conference on Circuit Theory and Design, Cork, Ireland, 2 September 2005; Volume 3, pp. III/101–III/104.
18. Acar, M.; Annema, A.; Nauta, B. Generalized Design Equations for Class-E Power Amplifiers with Finite DC Feed Inductance. In Proceedings of the 36th European Microwave Conference, Manchester, UK, 10–15 September 2006; pp. 1308–1311. [[CrossRef](#)]
19. Acar, M.; Annema, A.J.; Nauta, B. Analytical Design Equations for Class-E Power Amplifiers. *IEEE Trans. Circuits Syst. I Reg. Papers* **2007**, *54*, 2706–2717. [[CrossRef](#)]
20. Du, X.; Nan, J.; Chen, W.; Shao, Z. ‘New’ solutions of Class-E power amplifier with finite dc feed inductor at any duty ratio. *IET Circuits Devices Syst.* **2014**, *8*, 311–321. [[CrossRef](#)]
21. Fajardo, A.; de Sousa, F.R. Integrated CMOS class-E power amplifier for self-sustaining wireless power transfer system. In Proceedings of the 2016 29th Symposium on Integrated Circuits and Systems Design (SBCCI), Belo Horizonte, Brazil, 29 August–3 September 2016; pp. 1–6. [[CrossRef](#)]
22. Fajardo, A.; de Sousa, F.R. Simple expression for estimating the switch peak voltage on the class-E amplifier with finite DC-feed inductance. In Proceedings of the 2016 IEEE 7th Latin American Symposium on Circuits & Systems (LASCAS), Florianopolis, Brazil, 28 February–2 March 2016; pp. 183–186. [[CrossRef](#)]
23. Casallas, I.; Paez-Rueda, C.I.; Perilla, G.; Pérez, M.; Fajardo, A. Design Methodology of the Class-E Power Amplifier with Finite Feed Inductance—A Tutorial Approach. *Appl. Sci.* **2020**, *10*, 8765. [[CrossRef](#)]
24. Casallas, I.; Paez-Rueda, C.I.; Perilla, G.; Pérez, M.; Fajardo, A. Design of the Class-E Power Amplifier with Finite DC Feed Inductance under Maximum-Rating Constraints. *Appl. Sci.* **2021**, *11*, 3727. [[CrossRef](#)]
25. Gaudo, P.M.; Bernal, C.; Mediano, A. Output power capability of class-E amplifiers with nonlinear shunt capacitance. In Proceedings of the 2004 IEEE MTT-S International Microwave Symposium Digest (IEEE Cat. No.04CH37535), Fort Worth, TX, USA, 6–11 June 2004; Volume 2, pp. 891–894.
26. Sokal, N.O. Class-E RF power amplifiers. *QEX Commun. Quart* **2001**, *204*, 9–20.
27. Cantrell, W.H. Tuning analysis for the high-Q class-E power amplifier. *IEEE Trans. Microw. Theory Tech.* **2000**, *48*, 2397–2402. [[CrossRef](#)]
28. Selyutina, E.V.; Mindubaev, E.A. Capacitive Tuning of Adaptive Inductive Wireless Power Transfer System With a Class-E Power Amplifier. In Proceedings of the 2020 IEEE Conference of Russian Young Researchers in Electrical and Electronic Engineering (EIConRus), Moscow, Russia, 27–30 January 2020; pp. 2540–2544.
29. Selyutina, E.V.; Mindubaev, E.A. Effects Of Class E Power Amplifier Parameters On Output Power Of Inductive Wireless Power Transfer System With Capacitive Tuning. In Proceedings of the 2021 IEEE Conference of Russian Young Researchers in Electrical and Electronic Engineering (EIConRus), Moscow, Russia, 26–29 January 2021; pp. 2874–2878.
30. Grebennikov, A.; Sokal, N.O.; Franco, M.J. *Switchmode RF and Microwave Power Amplifiers*; Academic Press: Cambridge, MA, USA, 2012; pp. 260–276.
31. Sokal, N.; Mediano, A. Redefining the optimum RF Class-E switch-voltage waveform, to correct a long-used incorrect waveform. In Proceedings of the 2013 IEEE MTT-S International Microwave Symposium Digest (MTT), Seattle, WA, USA, 2–7 June 2013; pp. 1–3. [[CrossRef](#)]

32. Sabour, S.; Nazarpour, D.; Golshannavaz, S.; Choupan, R.; Yazdaninejadi, A.; Hassanifar, M. A new quasi-resonant switched capacitor multilevel inverter with the self-voltage balancing capability. *Int. Trans. Electr. Energy Syst.* **2020**, *30*, e12478. [CrossRef]
33. Van Wageningen, D.; Staring, T. The Qi wireless power standard. In Proceedings of the 14th International Power Electronics and Motion Control Conference EPE-PEMC 2010, Ohrid, Macedonia, 6–8 September 2010; pp. S15–S25.
34. *Introduction to the Power Class 0 Specification, Version 1.2.3*; Wireless Power Consortium, Inc.: Piscataway, NJ, USA, 2017.
35. Wireless Charging Coil Assembly, AWCCA-50N50. ABRACON. Available online: <https://abracon.com/Magnetics/wireless/AWCCA-50N50.pdf> (accessed on 12 May 2021).
36. Fiore, R. *ESR Losses in Ceramic Capacitors*; American Technical Ceramics: Huntington Station, NY, USA, 1999. Available online: [https://atceramics.com/userFiles/uploads/pdfs/esrlosses\\_appnote.pdf](https://atceramics.com/userFiles/uploads/pdfs/esrlosses_appnote.pdf) (accessed on 12 May 2021).
37. Cadence Design Systems, I. *Reference Guide PSpice*, 2nd online ed.; Cadence Design Systems, Inc.: Portland, OR, USA, 2000; pp. 172–196.
38. Power, J.; Lane, W. An enhanced SPICE MOSFET model suitable for analog applications. *IEEE Trans. Comput. Aided Des. Integr. Circuits Syst.* **1992**, *11*, 1418–1425. [CrossRef]
39. Stueckler, F.; Bueyuektas, K.; Noebauer, G. Introduction to Infineon’s Simulation Models Power MOSFETs. Infineon Technologies Austria AG. Available online: [https://www.infineon.com/dgdl/Infineon-ApplicationNote\\_PowerMOSFET\\_SimulationModels-AN-v01\\_00-EN.pdf?fileId=5546d46250cc1fd0151588db5ef1b18](https://www.infineon.com/dgdl/Infineon-ApplicationNote_PowerMOSFET_SimulationModels-AN-v01_00-EN.pdf?fileId=5546d46250cc1fd0151588db5ef1b18) (accessed on 12 May 2021).
40. IPI029N06N, Simulation Model. Infineon Technologies AG. Available online: <https://www.infineon.com/cms/en/product/power/mosfet/12v-300v-n-channel-power-mosfet/ipi029n06n/#!simulation> (accessed on 12 May 2021).